Stem Cell Reports
Resource
OPEN ACCESS

Reprogramming Captures the Genetic and Tumorigenic Properties of Neurofibromatosis Type 1 Plexiform Neurofibromas

Meritxell Carrió,[1] Helena Mazuelas,[1,9] Yvonne Richaud-Patin,[2,3,9] Bernat Gel,[1] Ernest Terribas,[1] Imma Rosas,[1] Senda Jimenez-Delgado,[2,3] Josep Biayna,[1,7] Leen Vendredy,[1,8] Ignacio Blanco,[4] Elisabeth Castellanos,[1] Conxi Lázaro,[5] Ángel Raya,[2,3,6,*] and Eduard Serra[1,*]

[1]Hereditary Cancer Group, Germans Trias i Pujol Research Institute (IGTP)-PMPPC-CIBERONC, Can Ruti Campus, Badalona, Barcelona 08916, Spain
[2]Center of Regenerative Medicine in Barcelona (CMRB), Hospitalet de Llobregat, Barcelona 08098, Spain
[3]Center for Networked Biomedical Research on Bioengineering, Biomaterials and Nanomedicine (CIBER-BBN), Hospitalet de Llobregat, Barcelona 08098, Spain
[4]Clinical Genetics and Genetic Counseling Program, Germans Trias i Pujol University Hospital (HUGTiP), Can Ruti Campus, Badalona, Barcelona 08916, Spain
[5]Hereditary Cancer Program, Catalan Institute of Oncology (ICO-IDIBELL-CIBERONC), L'Hospitalet de Llobregat, Barcelona 08098, Spain
[6]Institució Catalana de Recerca i Estudis Avançats (ICREA), Barcelona 08010, Spain
[7]Present address: Genome Data Science Group, Institute for Research in Biomedicine (IRB), Barcelona, Spain
[8]Present address: Peripheral Neuropathy Research Group, University of Antwerp, Antwerp, Belgium
[9]These authors contributed equally
*Correspondence: araya@cmrb.eu (Á.R.), eserra@igtp.cat (E.S.)
https://doi.org/10.1016/j.stemcr.2019.01.001

SUMMARY

Neurofibromatosis type 1 (NF1) is a tumor predisposition genetic disease caused by mutations in the *NF1* tumor suppressor gene. Plexiform neurofibromas (PNFs) are benign Schwann cell (SC) tumors of the peripheral nerve sheath that develop through *NF1* inactivation and can progress toward a malignant soft tissue sarcoma. There is a lack of non-perishable model systems to investigate PNF development. We reprogrammed PNF-derived *NF1*(−/−) cells, descendants from the tumor originating cell. These *NF1*(−/−)-induced pluripotent stem cells (iPSCs) captured the genomic status of PNFs and were able to differentiate toward neural crest stem cells and further to SCs. iPSC-derived *NF1*(−/−) SCs exhibited a continuous high proliferation rate, poor myelination ability, and a tendency to form 3D spheres that expressed the same markers as their PNF-derived primary SC counterparts. They represent a valuable model to study and treat PNFs. PNF-derived iPSC lines were banked for making them available.

INTRODUCTION

Neurofibromatosis type 1 (NF1) is a tumor predisposition genetic disease (VM & Riccardi, 1992) caused by the inheritance of a mutated copy of the *NF1* gene, a negative regulator of Ras (Ratner and Miller, 2015). The major disease features involve the nervous system, the skin, and the skeletal system. There is a great variability in the clinical expressivity of the disease, but the development of different tumors of the peripheral nervous system, such as cutaneous neurofibromas (CNFs), plexiform neurofibromas (PNFs) or, less frequently, malignant peripheral nerve sheath tumors (MPNSTs), constitute one of the hallmarks of the disease (Ferner, 2007).

PNFs are mainly developed in the context of NF1 and are thought to be congenital. They are identified in around 50% of NF1 individuals if MRI is used (Mautner et al., 2008). This tumor type constitutes a major source of morbidity (Prada et al., 2012) and, in some cases, undergoes malignant transformation (McCarron and Goldblum, 1998). Surgery is still the standard therapeutic option. However, complete resection can cause important functional deficiencies and sometimes can be unfeasible because of the size or location of the tumor (Packer and Rosser, 2002). Recently, the MEK inhibitor Selumetinib has been used in children with inoperable PNFs showing confirmed partial responses (Dombi et al., 2016).

Neurofibromas are composed of different cell types, mainly Schwann cells (SCs) and endoneurial fibroblasts, as well as perineurial cells and infiltrating immune cells, all embedded in an abundant collagen-rich extracellular matrix (Krone et al., 1983; Peltonen et al., 1988). PNFs arise through a biallelic inactivation of the *NF1* gene (Däschner et al., 1997; Hirbe et al., 2015; Kluwe et al., 1999; Rasmussen et al., 2000). Only neurofibroma-derived SCs bear this *NF1* inactivation (Kluwe et al., 1999; Li et al., 2016; Maertens et al., 2006; Muir et al., 2001; Serra et al., 2000). Like CNFs, different PNFs arising in the same individual bear different somatic *NF1* mutations (Pemov et al., 2017). Also, like CNFs (Garcia-Linares et al., 2011), no recurrent gross genomic alterations or recurrent point mutations have been identified in PNFs besides the involvement of chromosome 17 in the inactivation of the *NF1* locus (Beert et al., 2011; Carrió et al., 2018; Miller et al., 2009; Pemov et al., 2017). PNF progression to malignancy often occurs through the formation of a pre-malignant lesion termed atypical neurofibroma, which involves the additional loss of the *CDKN2A/B* locus (Beert et al., 2011; Higham et al., 2018). It has been shown in one case (Hirbe et al., 2015) that somatic *NF1* inactivating mutation is shared by PNF

and their subsequent MPNST and metastasis, linking the PNF and MPNST cell of origin.

Different models for PNFs have been developed, both *in vitro* (primary cells, immortalized cells, 3D culture models) and *in vivo* (genetically modified mouse models). Primary SC cultures from PNFs have been established (Wallace et al., 2000). However, these cultures are perishable after several passages, limiting their use for molecular and cellular analyses that require large amounts of cells. To overcome this problem, immortalized cell lines have been generated (Li et al., 2016), but inextricably alter the biological status of the cells. These cells have also been used to generate 3D models (Kraniak et al., 2018) to better recapitulate the natural PNF environment of SCs. In addition, different genetically modified animal models using the Cre/lox system to ablate *NF1* in specific cell stages of the neural crest stem cells (NCs, for simplicity)-SC axis during development have been generated that develop PNFs (reviewed in Buchstaller et al., 2012). Furthermore, Chen et al. (2014) established a non-germline model of PNF, consisting of the transplantation of *Nf1*-deficient embryonic dorsal root ganglia/nerve root neurosphere cells to sciatic nerves of nude mice.

Another way of obtaining imperishable cell-based model systems is the generation of induced pluripotent stem cells (iPSCs) (Takahashi and Yamanaka, 2006). iPSCs have been generated to model hereditary cancer syndromes (Papapetrou, 2016), like Fanconi anemia (Raya et al., 2009). iPSCs for NF1n have also been developed (Anastasaki et al., 2015; Larribere et al., 2015; Wegscheid et al., 2018). However, as for most other cancer syndromes, NF1 iPSCs have been generated from patient fibroblasts and not directly from cells of the associated tumors.

iPSC technology has been used to reprogram cancer cells, encountering different obstacles, such as their chromosomal and genomic composition or the necessity of remodeling their epigenetic state. Another limiting factor is the cell type to be reprogrammed. These aspects make the efficiency of generating iPSCs from cancer cells low (Kim and Zaret, 2015). Despite the low efficiency, there are several examples of iPSCs generated from cancer cells (Pan et al., 2017), mainly from established cancer cell lines (Bernhardt et al., 2017) and much less common from primary tumors (Kim et al., 2013; Kotini et al., 2017). However, the generation of iPSCs from benign tumors or pre-malignant lesions has been less explored (Papapetrou, 2016). To generate a non-perishable cell-based model system that recapitulates the genetic content and tumorigenic properties of NF1 benign PNFs, we generated iPSCs directly from PNF-derived primary cells. These iPSCs were differentiated to NCs and further to SCs. *NF1*(−/−) SCs obtained from PNF-derived iPSCs were extensively characterized and compared with primary *NF1*(−/−) SCs derived from primary tumors.

RESULTS

Generation of PNF-Derived iPSC Lines

We obtained five different PNFs (code-named 3PNF, 5PNF, 6PNF, 7PNF, and 13PNF) from five independent patients diagnosed of NF1 according to standard diagnostic criteria (DeBella et al., 2000). For most of them, histological information is available (Carrió et al., 2018). PNFs are composed of different cell types, mainly SCs and endoneurial fibroblasts. SCs within PNFs are the only cells bearing the two *NF1* alleles inactivated, one by a constitutional mutation shared by all cells of the individual, and the other by a somatic mutation specific for each PNF. Our intention was to create an imperishable cell-based model resource by reprogramming *NF1*(−/−) cells present in PNF descendants from the cell originating them. In addition, we planned to obtain *NF1*(+/−) isogenic iPSCs from the same tumors. We first determined the *NF1* germline mutation of each patient by next-generation sequencing panel analysis (Castellanos et al., 2017) and also the *NF1* somatic mutation of each excised PNF (Table 1; Figure S1). *NF1*(−/−) iPSCs were generated either from pure cultures of PNF-derived *NF1*(−/−) SCs (Serra et al., 2000) or directly from a short culture of PNF-dissociated cells. *NF1*(+/−) iPSCs were obtained by reprogramming either cultures of PNF-derived *NF1*(+/−) endoneurial fibroblasts, directly from PNF-dissociated cells or from skin-derived fibroblast cultures of the same patients (see Table S1 for details). Reprogramming to pluripotency was induced by retrovirus- and/or Sendai virus-mediated transduction (Ban et al., 2011; Takahashi and Yamanaka, 2006) of the patient-derived cells. Table 1 summarizes information on patient (sex, age, and germline mutation), tumor (diagnostic and *NF1* somatic mutation), and iPSC (name and banking information). Further reprogramming information is summarized in Table S1.

Overall, we generated seven genetically different iPSC lines from five independent NF1 patients. We were able to isolate two independent *NF1*(−/−) iPSCs, bearing the constitutional and somatic *NF1* mutations, from five distinct PNFs. From all five patients we obtained *NF1*(+/−) iPSCs bearing only the constitutional mutation. Thus, from two different tumors, 3PNF and 5PNF, we were able to generate isogenic iPSC lines bearing two distinct *NF1* genotypes: *NF1*(+/−) and *NF1*(−/−) (Table 1).

Characterization of PNF-Derived iPSC Lines

After confirming the *NF1* genetic status, selected iPSC clones representing each patient and *NF1* genotype were further expanded and characterized. Figure 1 illustrates the characterization of the isogenic iPSC lines derived from 3PNF and 5PNF; the characterization of the remaining banked iPSC lines is shown in Figure S2. We selected

Table 1. Patient, Tumor, and iPSC Line Information

Patient Information				Tumor Information			iPSC Lines Generated	
Patient ID	Sex	Age (at PNF Resection)	NF1 Germline Mutation	Tumor ID	Diagnostic	NF1 Somatic Mutation	iPSC Line (Named in the Paper)	iPSC Line (Banking Name)
3	XX	8	c.3943C > T; p.Gln1315*	3PNF	PNF with diffuse extraneural invasion	LOH (HR) whole ch.17q	3PNFiPS(NF1+/−)	3PNF_FiPSsv_PM
							3PNFiPS(NF1−/−)	3PNF_SiPSsv_MM
5	XY	10	intragenic deletion (E16-35)	5PNF	PNF with diffuse extraneural invasion	LOH (3.8Mb del)	5PNFiPS(NF1+/−)	5PNF_TDiPSsv_PM
							5PNFiPS(NF1−/−)	5PNF_TDiPSsv_MM
6	XX	33	c.2946delT; p.Leu983*	6PNF	PNF with diffuse extraneural invasion	c.2033dupC; p.Ile679Aspfs*21	6PNFiPS(NF1+/−)	6PNF_SiPSrv_PM
7	XX	66	c.2033dupC; p.Ile679Aspfs*21	7PNF	PNF with diffuse extraneural invasion	LOH (1.4Mb del)	7PNFiPS(NF1+/−)	7PNF_TDiPSrv_PM
13	XY	14	c.1318C > T; p.Arg440*	13PNF	PNF with diffuse extraneural invasion	LOH (HR) whole ch.17q	13PNFiPS(NF1+/−)	not banked

LOH, loss of heterozygosity; HR, homologous recombination. The link below will take you to the Spanish National Stem Cell Bank-Institute of Health Carlos III, where the iPSC lines have been deposited to be able to be distributed. http://www.eng.isciii.es/ISCIII/es/contenidos/fd-el-instituto/fd-organizacion/fd-estructura-directiva/fd-subdireccion-general-investigacion-terapia-celular-medicina-regenerativa/fd-centros-unidades/fd-banco-nacional-lineas-celulares/fd-lineas-celulares-disponibles/lineas-de-celulas-iPS.shtml.

clones that displayed a compact embryonic stem cell-like morphology, were positive for alkaline phosphatase staining, and expressed high levels of pluripotency-associated transcription factors and surface markers (Figures 1A and 1B). Moreover, selected clones showed pluripotent differentiation ability *in vitro* and *in vivo* (teratoma formation), demethylation of *POU5F1* and *NANOG* promoters, and karyotype stability after more than 15 passages (Figures 1C–1F and S2). It is worth noting that 5PNFiPS(−/−) carried a chromosomal translocation (karyotype: 46,XYt(17; 22)(q11.2; q13.3)) also present in the parental reprogrammed SCs, as the cause of *NF1* somatic inactivation (Figure S2G). Finally, we confirmed by PCR-based DNA fingerprinting analysis that the iPSC lines generated genetically matched their parental tumors (Table S2). As expected, the levels of neurofibromin were reduced in *NF1*(+/−) iPSCs compared with control *NF1*(+/+) pluripotent cells, and were absent in *NF1*(−/−) iPSCs (Figure 2G). Altogether, these data demonstrated that we successfully generated iPSCs from PNF-derived *NF1*(+/−) and *NF1*(−/−) cells, and indicated that reduced levels or even absence of neurofibromin did not appear to compromise somatic cell reprogramming to pluripotency, maintenance, or differentiation capacity of iPSCs.

PNF-Derived *NF1*(−/−) iPSCs Exhibit a Higher Proliferation Rate Than Control Pluripotent Cells

It has been shown that *NF1*-deficient cells exhibit a higher proliferation rate than their cellular counterparts carrying one or two wild-type copies of the *NF1* gene (Kim et al., 1995, 1997; Rosenbaum et al., 1995). Consistent with this, we noticed that cultures of *NF1*(−/−) 3PNFiPS and 5PNFiPS needed to be split more frequently than control iPSCs or human embryonic stem cells (hESCs) maintained in parallel. To quantify the effect of the *NF1* status on iPSC proliferation rate, we used a flow cytometry-based Click-iT EdU assay. We compared PNF-derived *NF1*(+/−) or (−/−) iPSC lines with control *NF1*(+/+) pluripotent stem cells (PSCs). Control cells included iPSCs from skin fibroblasts of a healthy donor (FiPS cell line) and embryonic stem cells (ES4 cell line). On average, *NF1*(−/−) 3PNFiPS and 5PNFiPS cell lines exhibited a 10%–15% increase in cell proliferation rate compared with control PSCs (Figure 2H). *NF1*(−/−) iPSCs also exhibited a higher proliferation rate than *NF1*(+/−) iPSCs ($p < 0.05$). These results indicate that cell proliferation rate in PSCs, as is the case for somatic cells, is influenced by neurofibromin activity.

PNF-Derived iPSCs Capture the Genomic Status of Their Cell of Origin

We extensively characterized the genomic content of the different iPSC lines generated from PNFs. We performed cytogenetic karyotyping, exome sequencing, and molecular karyotyping by SNP array analysis comparing tumors, *NF1*(−/−) SC and *NF1*(+/−) fibroblast cultures and iPSCs. All samples were 2n according to the cytogenetic and molecular karyotypes (Figures 1F, 2A, S2, and S3). As previously observed in CNFs (Garcia-Linares et al., 2011), the only genomic alterations present resulted from the somatic inactivation of the *NF1* gene, in some cases affecting the structure of chromosome 17q (Figures 2 and S3) (Carrió et al., 2018). Gross somatic mutations affecting the *NF1*

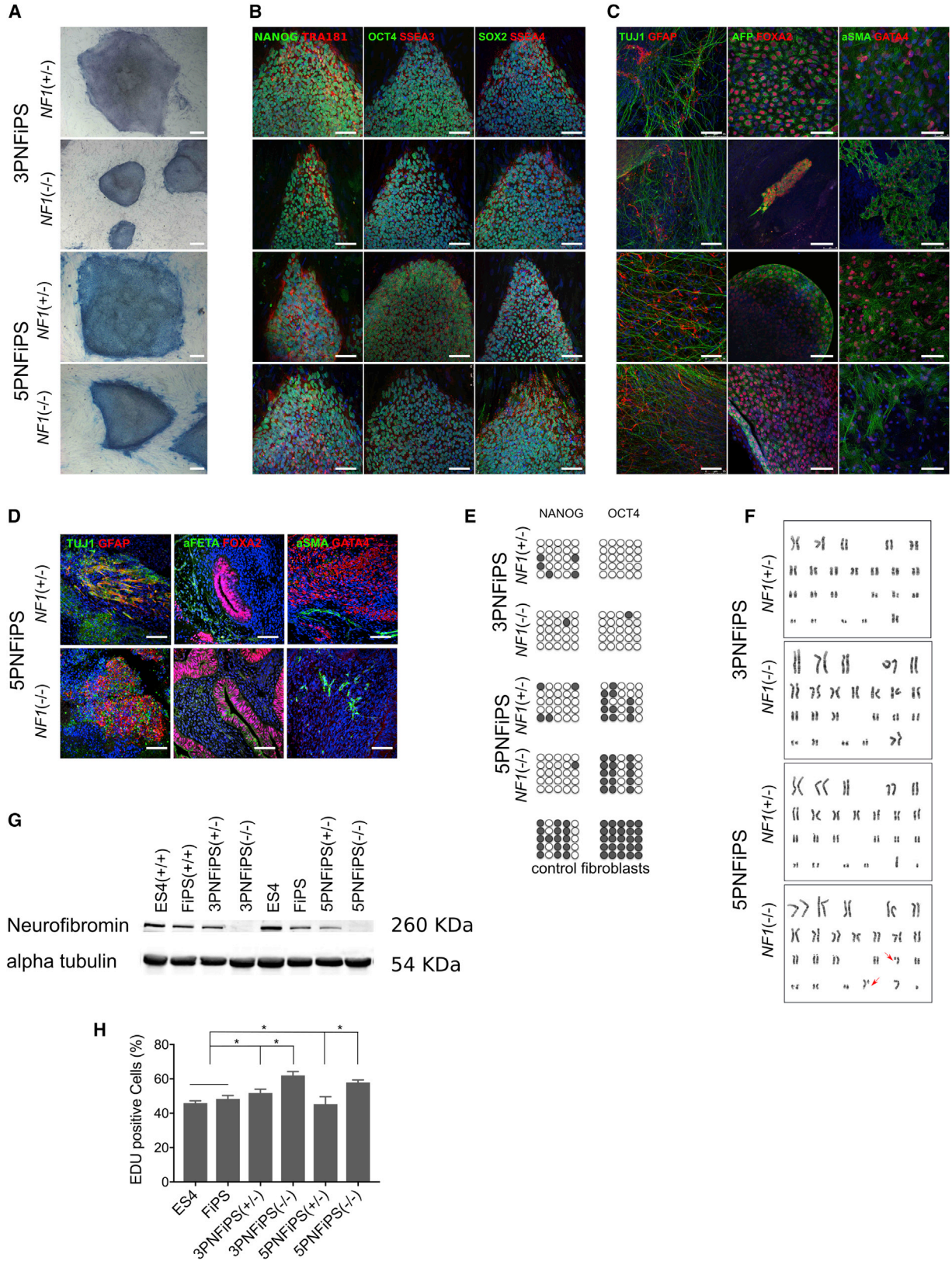

(legend on next page)

gene were found in four of the tumors and consisted in either large deletions of 1.4 Mb (7PNF) and 3.8 Mb (5PNF), both involving the *NF1* and *SUZ12* genes, or homologous recombination (3PNF and 13PNF) generating loss of heterozygosity (LOH) in almost the entire 17q arm (Figure 2B) and bringing the constitutional *NF1* mutation into homozygosity, as described previously (Serra et al., 2001; Steinmann et al., 2009). Somatic *NF1* inactivation in 6PNF was due to a point mutation (Table 1; Figure S1). The same somatic *NF1* inactivation was shared by PNF and its derived *NF1*(−/−) SC culture, but was not present in fibroblast cultures or in *NF1*(+/−) iPSCs (Figures 2 and S3). We also performed exome sequencing to identify the presence of small pathogenic variants. On average, we identified the presence of ten additional point mutations in the whole exome of PNF-derived iPSCs that were not present in PNFs or primary SC cultures (Figure 2C; Table S3). The low number of mutations is consistent with the reprogramming and clonal expansion of a cell already containing these mutations, which would not be detectable in the bulk cell population of PNFs or primary SC cultures. None of the identified somatic point mutations was recurrent among the five PNFs (data not shown for 13PNF). These results are in agreement with data from recent exome analysis of PNFs and CNFs (Gosline et al., 2017; Pemov et al., 2017).

Neural Crest Differentiation of PNF-Derived iPSCs

We posit that PNF-derived iPSCs constitute a non-perishable cell-based experimental system that should facilitate the identification of the PNF cell of origin as well as the development of therapeutic strategies against these types of tumors. Thus, we next set out to differentiate PNF-derived iPSCs toward the NC-SC axis. To generate NCs, we used a previously described differentiation protocol that employs chemically defined medium to activate Wnt signaling while inhibiting Activin/Nodal/transforming growth factor β signaling (Lee et al., 2007; Menendez et al., 2013) (see Supplemental Experimental Procedures for details).

Control PSCs, as well as all *NF1*(+/−) and *NF1*(−/−) PNF-derived iPSC lines tested, successfully differentiated toward NC cells when applying this protocol. Approximately 12 days after NC induction, cells adopted a stellate morphology typical of NCs (Figure 3A), which was maintained throughout the passages. To characterize the generated NCs we performed flow cytometry analysis using two specific NC markers, p75 (*NGFR*) and HNK1 (Lee et al., 2010), at early (7–10 days, passage 1) and late (>20 days, passage 4–5) differentiation stages (Figure 3B). Although both markers were heterogeneously expressed in early passages, NCs from both control and PNF-derived iPSCs homogeneously co-expressed high levels of p75 and HNK1 at later differentiation stages, indicating a clear NC identity. NCs cultured under these specific conditions could be maintained as a stable, self-renewing population for up to 20 passages without losing NC identity (see below), enabling the freezing and cryopreservation of NC batches for subsequent differentiation assays.

NC identity was further confirmed by immunofluorescence (Figure 3C) and qRT-PCR (Figure 3D) analyses of the NC markers SOX10, p75, and AP2. qRT-PCR analyses also showed that PSC-derived NCs did not express the pluripotency-associated marker OCT4 (*POU5F1*), or the SC lineage-specific marker S100b, present in PNF-derived SCs (Figure 3D). Moreover, we also functionally tested NC biological capacities such as migration and differentiation potential. A scratch assay showed the ability of all NCs (control and PNF derived) to start migrating already at 6 h and to be able to close the scratch in less than 24 h (Figure S4A). Furthermore, PSC-derived NCs were able to undergo further differentiation into NC-derived cell types, such as peripheral neurons and melanocytes (Figure S4B), confirming their NC multi-lineage differentiation ability.

Figure 1. Characterization of PNF-Derived iPSC Lines

(A) Morphology and alkaline phosphatase staining of 3PNF and 5PNF iPSC colonies. Scale bars, 100 μm.

(B) Characterization of pluripotency markers. Representative images of 3PNF and 5PNF iPSC colonies stained positive for the pluripotency-associated markers NANOG, OCT4, and SOX2 (in green), and TRA-1-81, SSEA3, and SSEA4 (in red). Scale bars, 100 μm.

(C) *In vitro* differentiation potential of 3PNF and 5PNF iPSC lines. Generation of cell derivatives of the three primary germ layers including ectoderm (TUJ1 in green and GFAP in red), endoderm (AFP in green and FOXA2 in red) and mesoderm (SMA in green and GATA4 in red). Scale bars, 100 μm.

(D) Teratoma formation from 5PNF iPSC, showing their differentiation toward ectoderm (TUJ1 in green and GFAP in red), endoderm (AFP in green and FOXA2 in red) and mesoderm (SMA in green and GATA4 in red). Scale bars, 100 μm.

(E) Bisulphite sequencing showing demethylation of *NANOG* and *POU5F1* promoters in the 3PNF and 5PNF iPSC lines.

(F) Karyotype of 3PNF and 5PNF iPSC lines at passage 20.

(G) Western blot analysis showing the absence of neurofibromin in 3PNFiPS(−/−) and 5PNFiPS(−/−). The human embryonic stem cell (hESC) line ES4 and a control iPSC line generated from foreskin fibroblasts (FiPS), both *NF1*(+/+), were used as control cell lines.

(H) Proliferation capacity of 3PNF and 5PNF iPSC lines assessed by Click-iT EdU Flow Cytometry Assay. Double-positive cells (in S phase) are represented in the graph. Bars represent means from three independent experiments.*$p < 0.05$ (unpaired t tests).

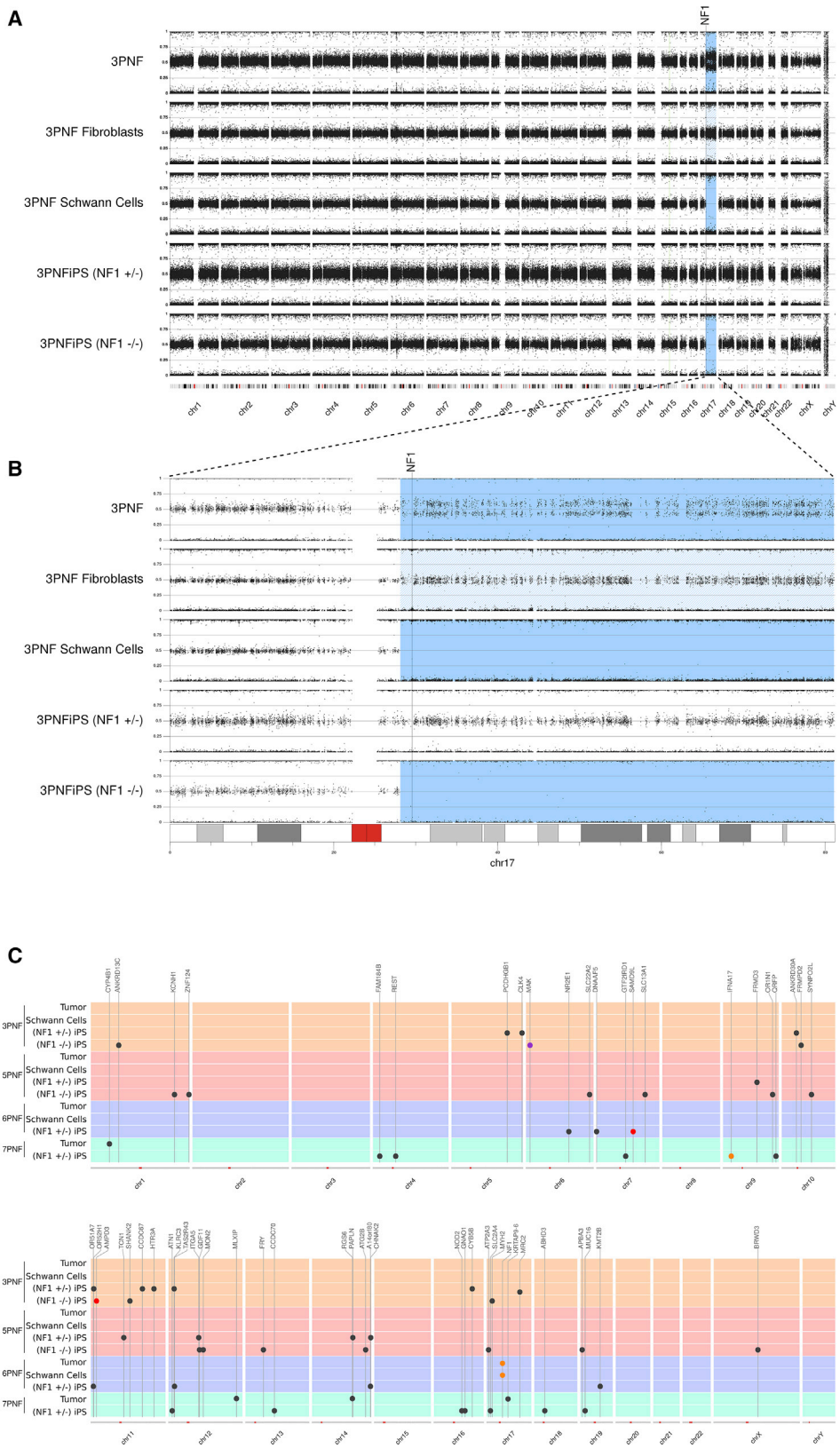

(legend on next page)

SC Differentiation of PNF-Derived NCs

We then set up an SC differentiation protocol starting from the established NCs. We differentiated NCs from control FiPS and PNF-derived iPSC lines into SCs (Figure 4A) (see Supplemental Experimental Procedures). The differentiation process was monitored by immunocytochemistry and qRT-PCR analysis of various markers of the NC-SC lineage at different time points (7, 14, and 30 days).

After 7 days under SC differentiation conditions, NCs from *NF1*(+/+) control FiPS already changed morphology, becoming more elongated. This phenotype progressed over time until reaching the typical bipolar spindle-like morphology of SCs between 14 and 30 days of differentiation (Figure 4B). SC markers such as p75 and S100b were expressed homogenously in the culture throughout the whole differentiation process (Figure 4B). qRT-PCR analysis confirmed expression of NC-SC lineage-specific markers throughout the differentiation process (Figure 4D). *NGFR* and *SOX10*, two key regulators of NC formation and SC fate determination, persisted during the entire differentiation process. Expression of SC precursor markers such as *CDH19*, *ITG4A*, and *MPZ* had a remarkable increase after 7 days of differentiation. *GAP43* was also highly expressed. SC markers such as *PLP*, *PMP22*, and S100b were already detected after 1 week of differentiation and reached maximum expression by day 30. *EGR2* (*KROX20*), a master regulator for myelinating SC was detected already in NCs and had a peak at 30 days of differentiation, as reported previously (Jessen and Mirsky, 2005; Reiprich et al., 2010) (Figure 4D).

At 7 days of differentiation *NF1*(−/−) NCs resembled control *NF1*(+/+) cells, both morphologically and according to SC marker expression (p75 and S100b) (Figure 4C). After 14 days of differentiation, *NF1*(−/−) cells already acquired the slender, elongated morphology of SCs. However, whereas control *NF1*(+/+) cultures progressively stopped proliferation, maintaining a homogeneous expression of SC markers, *NF1*(−/−) cells continued to exhibit a high proliferation capacity and heterogeneously expressed some of the markers, such as S100b (Figure 4C). This altered differentiation process of *NF1*(−/−) SCs was also observed by qRT-PCR analysis (Figure 4E). While markers of the NC-SC lineage were expressed in differentiation *NF1*(−/−) SC cultures, those markers related to SC maturation were not maintained through the differentiation process compared with control *NF1*(+/+).

NF1(−/−) Differentiating SCs Exhibited a Continuous High Proliferation Rate and a Lack of Myelination Capacity

NF1(−/−) differentiating SCs proliferated so much during differentiation experiments that cultures were generated with a high cell density and a natural tendency to form sphere-like structures visible to the naked eye. Spheres grew either attached to the plate surface or as free-floating cultures resembling 3D spheroids (Figures 5A and 5B). We quantified the proliferation capacity of differentiating SCs by Ki-67 immunostaining (Figure 5C), confirming a statistically significant higher proliferation rate in *NF1*(−/−) cells, both at 7 and at 30 days of SC differentiation, compared with control *NF1*(+/+) and *NF1*(+/−) cell lines (Figure 5D).

In addition to the proliferation rate of differentiating SCs, we also tested their ability to myelinate axons. *NF1*(+/+) FiPS-derived SCs, co-cultured with rat dorsal root ganglion (DRG) neurons in the presence of myelinating medium, were capable of associating and myelinating peripheral neuron axons, as demonstrated by the co-localization of S100b/myelin protein zero (MPZ)-positive cells with neuron-specific tubulin (TUJ1)-positive axons (Figure 5E). We identified fragments of myelinated axons longer than 400 μm in three independent experiments (Figure S5). These functional assays confirmed the myelinating capacity of FiPS-derived SCs and validated the protocol used to differentiate NCs into SCs. However, when we co-cultured *NF1*(−/−) iPSC-derived SCs with DRG neurons, they kept proliferating during the assay and were not able to properly associate and form myelinating axons, neither cells growing in monolayer nor sphere-forming cells, as happens in PNFs (Figure 5F). *NF1*(−/−) differentiating SCs generated either spheres or wide lanes of organized cells. In addition, *NF1*(−/−) cells expressed the

Figure 2. Genomic Characterization of PNFs, Primary Cells, and Generated iPSCs

(A) B allele frequency (BAF) data from SNP array analysis characterizing the genomic structure of five samples associated with 3PNF tumor; fibroblasts; PNF-derived Schwann cells; 3PNFiPS(+/−) and 3PNFiPS(−/−). The genome of all samples was mostly 2n, denoted by a BAF signal around 0.5. A blue shaded region indicates somatic copy neutral (CN)-loss of heterozygosity (LOH).

(B) A detailed view of BAF for chromosome 17. Somatic *NF1* inactivation was produced by mitotic recombination generating CN-LOH in 17q and the reduction to homozygosity for the constitutional *NF1* mutation. LOH is observed in 3PNF and in 100% of cells in 3PNF-derived Schwann cells and in 3PNFiPS(−/−). Fibroblast primary culture (3PNF fibroblasts) is an early passage and still exhibit a residual LOH due to the presence of "contaminating" tumor SCs.

(C) Summary of somatic exonic variants identified by exome sequencing. All samples associated with a PNF are represented by wide horizontal line of the same color covering all chromosomes. Color dots indicate the type of genetic variant: missense (black), frameshift (orange), in-frame deletion (purple), and non-sense (red). Position of genes containing the variants is marked with vertical lines.

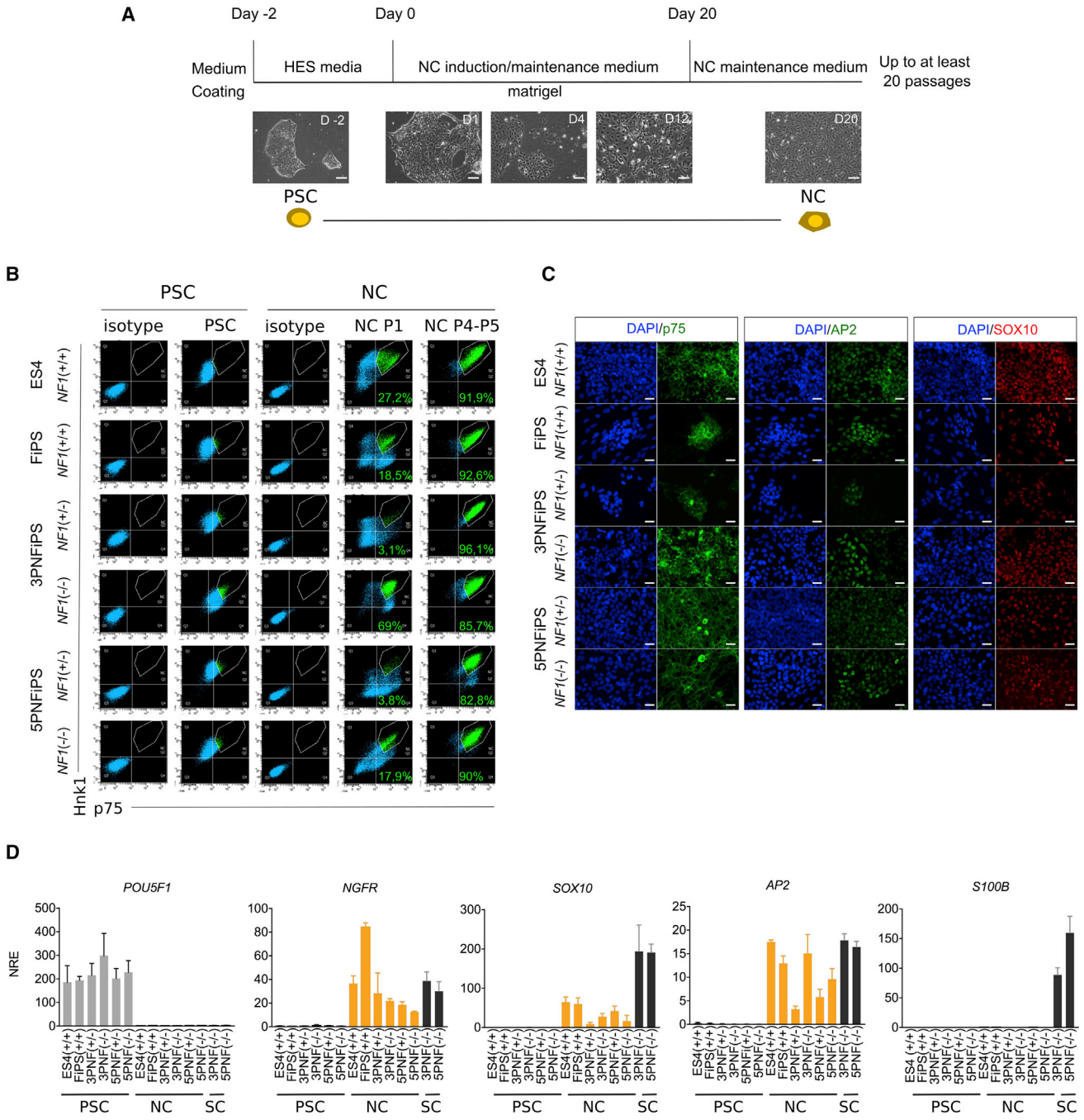

Figure 3. PNF-Derived iPSCs Correctly Differentiate into NCs

(A) Schematic representation of the protocol used for differentiating iPSCs into NCs. Control (ES4 and FiPS) and PNF-derived iPSCs were seeded on Matrigel and cultured in NC induction medium for 20 days (see Supplemental Experimental Procedures). Representative bright-field images during the differentiation process over time (in days, D) are shown. PSC, pluripotent stem cell. Scale bar, 50 μm.

(B) Flow cytometry analysis for p75 and Hnk1 before and after NC differentiation. The percentage of double p75 and Hnk1-positive cells is shown inside the graph. P1, passage 1; P4-5, passages 4–5.

(legend continued on next page)

neuronal marker TUJ1, complicating the analysis. Since TUJ1 was not expressed by *NF1*(+/+) differentiating SCs in the co-culture assay, we analyzed PNF-derived primary SC cultures and found that they also expressed TUJ1 (Figure 5G).

Sphere-Forming SCs from *NF1*(−/−) iPSCs Recapitulate the Expression Pattern of Their PNF-Derived Primary SC Counterparts

To have a better idea to which extent sphere-forming *NF1*(−/−) differentiating SCs from PNF-derived iPSCs recapitulated the expression of their primary PNF counterparts, we compared the expression of SC markers in *NF1*(−/−) spheres at 30 days of differentiation with the expression of their parental PNF-derived primary SCs (Figure 6A). In contrast to the heterogeneous expression of SC markers (s100b) exhibited by differentiating SCs growing in monolayer (Figure 4C), sphere-forming SCs homogeneously expressed all markers tested. When we analyzed the expression of p75, s100b, SOX10, GAP43, and PLP by immunofluorescence, the expression pattern of PNF-derived SCs and sphere-forming SCs were strikingly similar (Figure 6A).

Sphere-forming SCs bore the same genetic and genomic content as their primary SC counterparts and recapitulated both a high proliferation rate and the same expression pattern in a homogeneous manner. Taking everything together, *NF1*(−/−) iPSC-derived spheres represent a valuable experimental model to study PNF formation, and to test potential therapeutic options *in vitro* (Figure 6B).

DISCUSSION

There exists a lack of imperishable cell-based systems to model benign tumor progression and assay therapeutic strategies. PNFs are benign SC tumors of the peripheral nervous system associated to NF1 that can progress toward a malignant soft tissue sarcoma. We have generated *NF1*(−/−) iPSC lines directly from PNFs, sharing the same constitutional and somatic *NF1* mutations as the cell originating them. We also generated five independent *NF1*(+/−) iPSCs from five PNFs, two being isogenic to the *NF1*(−/−) iPSC lines established. These cells have the genetic and genomic content of their parental primary cells, and can be differentiated toward NCs and further to SCs. SCs derived from *NF1*(−/−) iPSCs exhibit a high proliferation rate, show poor ability to myelinate, and show a tendency to form spheres in culture that resemble PNFs and preserve the same expression marker profile of the NC-SC axis as their parental *NF1*(−/−) primary SCs.

iPSC technology has been used to reprogram cancer cells, encountering different obstacles, like the chromosomal and genomic composition of cancer cells or the necessity of remodeling their epigenetic state. The *NF1*(−/−) iPSCs described here may have overcome these problems since they have been generated from benign tumors. Reprogramming technology has been previously used to model hereditary cancer syndromes (Papapetrou, 2016), NF1 among them (Anastasaki et al., 2015; Larribere et al., 2015; Wegscheid et al., 2018), but never from cells of the associated tumors. PNFs have the potential to progress to malignancy. In this regard, we believe that these iPSCs could constitute an excellent model for investigating tumor progression when combined with existing DNA-editing tools (CRISPR-Cas9) to better identify the genetic and epigenetic changes required for malignant transformation.

Even though the relatively low number of samples complicates drawing strong conclusions, we noticed that the efficiency of generating *NF1*(−/−) iPSC lines from PNFs (also *NF1*(+/−)) varied depending on the tumor and on the starting cell type. Different factors could be involved, such as the culture conditions used, the different reprogramming efficiency of distinct cell types (reviewed in Ebrahimi, 2015) or the age of the PNF donor, although all these aspects would need to be further explored.

Whereas *NF1*(+/+) differentiating SCs progressively stopped proliferation, maintained a homogeneous expression of SC markers, and had the capacity to myelinate axons, *NF1*(−/−) cells continued exhibiting a high proliferation capacity and heterogeneously expressed S100b during differentiation, and exhibit a poor ability to myelinate axons. These results are consistent with the biological status of SCs within PNFs. The exact mechanism and role of the *NF1* gene in relation to the altered SC differentiation is an exciting topic for further research.

The PNF-resembling spheres generated by the high proliferation capacity of differentiating SCs from PNF-derived *NF1*(−/−) iPSCs constitute a very promising non-perishable model for PNFs, even more so taking into account that currently there is no tumoroid model generated directly from primary PNF cells. An *in vitro* 3D PNF model

(C) Immunocytochemistry analysis showing that both control (ES4 and FiPS) and PNF-derived iPSCs differentiated to NCs (passage 5) express p75 (green), AP2 (green), and SOX10 (red). DAPI was used to stain cell nuclei. Scale bar, 50 μm.

(D) qRT-PCR expression analysis of pluripotent (*POU5F1*), NC (*NGFR, SOX10, AP2*), and SC (*S100B*) markers, in pluripotent cells (PSCs), PSCs differentiated to NCs and PNF-derived SCs. qRT-PCR values are expressed as the mean normalized relative expression (NRE) ± SEM from three independent differentiation experiments.

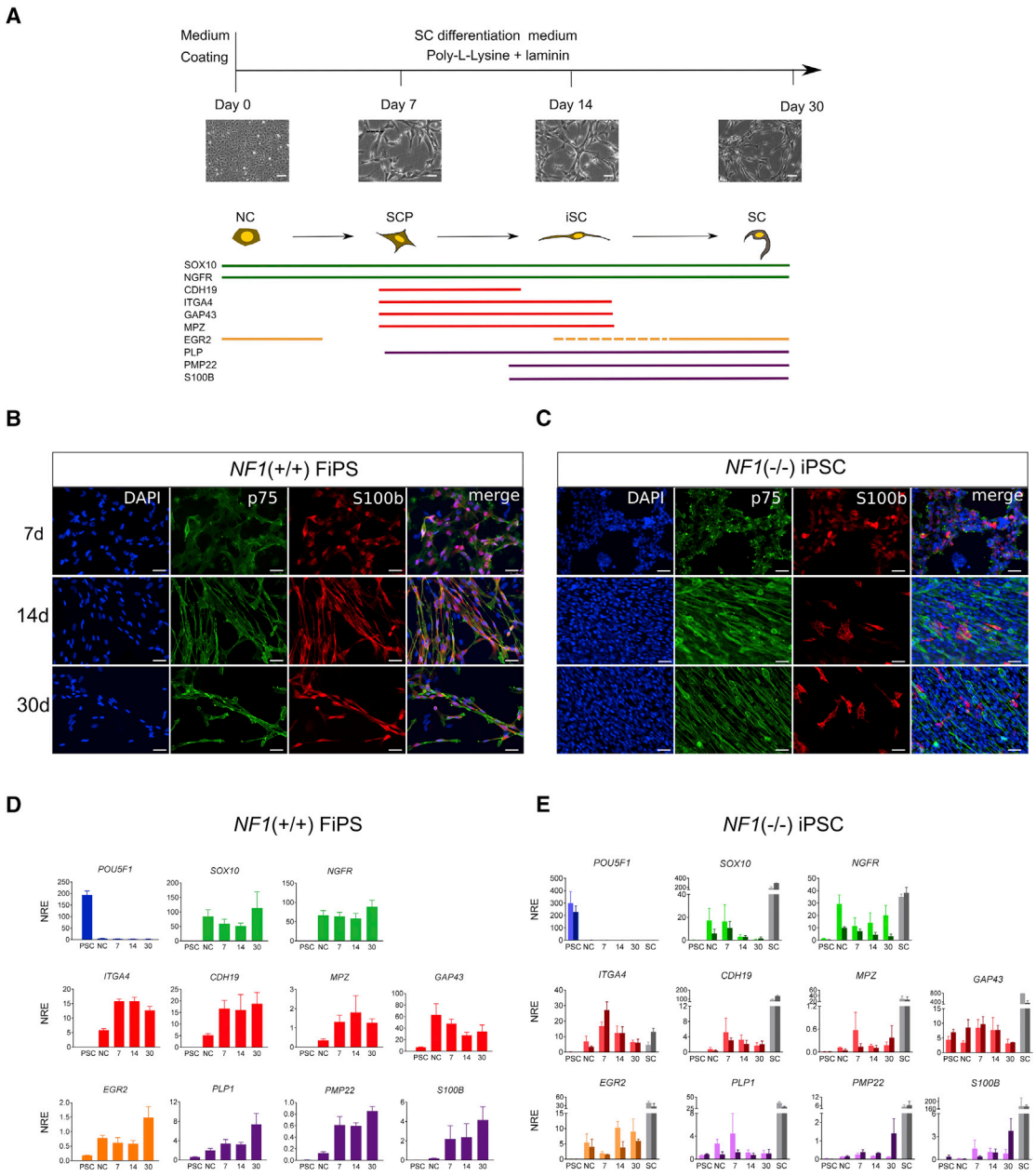

Figure 4. Schwann Cells Differentiation of iPSC-Derived NCs

(A) Top: schematic representation of the protocol used for differentiating NCs to Schwann cells (SCs). NCs were seeded on poly-L-lysine and laminin-coated plates and cultured in SC differentiation medium (see Supplemental Experimental Procedures). After 7, 14, and 30 days, SC differentiation was monitored by qRT-PCR and immunocytochemistry analysis. Representative bright-field images during the differentiation process from a control cell line are shown. Scale bars, 50 μm. Bottom: diagram showing the expression of markers associated with the NC-SC lineage. The colored horizontal bars represent the temporal window during differentiation when the corresponding marker is expressed *in vivo*, according to the literature (Jessen and Mirsky, 2005). SCP, Schwann cell precursor; iSC, immature Schwann cells (iSCs).

(B and C) Immunocytochemical analysis for S100b and p75 at different stages of SC differentiation (7, 14, and 30 days) in control *NF1*(+/+) FiPS (B) and 3PNFiPS(−/−) cells (C). DAPI was used to stain cell nuclei. Scale bars, 50 μm.

(D and E) qRT-PCR in control *NF1*(+/+) FiPS (D) and *NF1*(−/−) iPSCs (E) at five different time points during differentiation: pluripotent stage (PSC), neural crest stage (NC) and at 7, 14, or 30 days of SC differentiation. For *NF1*(−/−) iPSC graphs (E): light bar represents SC differentiation for 3PNF and dark bar for 5PNF. As control cells for marker expression, primary SC cultures (gray bars) from 3PNF (light gray) and 5PNF (dark gray) were used. Values are expressed as the mean NRE ± SEM from three independent differentiation experiments.

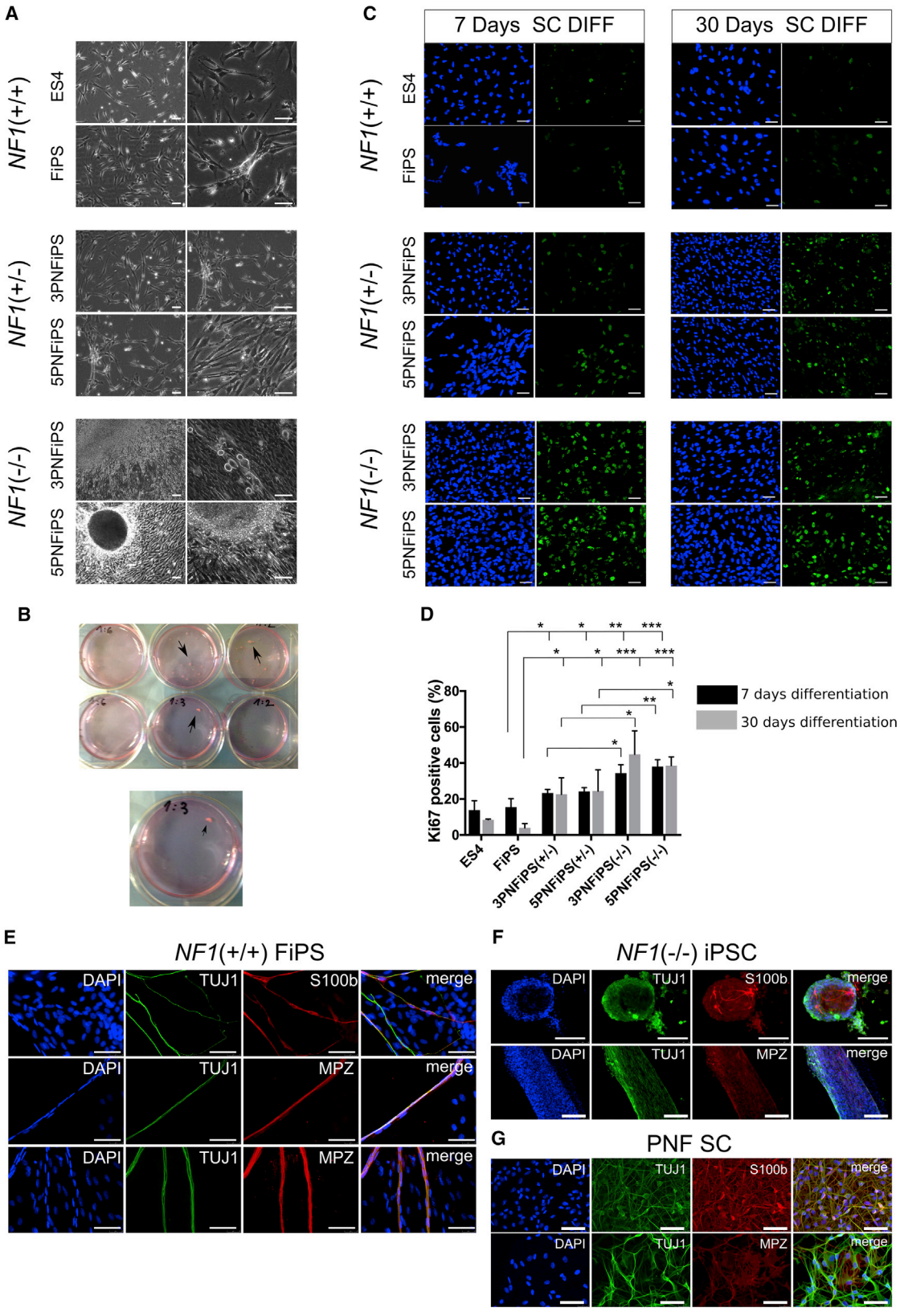

(legend on next page)

will facilitate the testing of therapeutic agents in a PNF-resembling environment before jumping to an *in vivo* model, although further development will be necessary.

In the field of NF1 research, there is still an open debate regarding the cell of origin of neurofibromas (Buchstaller et al., 2012). PNFs are thought to be congenital but the identity and biological capacity of the cell type that receives the inactivation of *NF1* is still not completely understood. Essential information has been obtained from the different genetically modified mouse models that develop PNFs in which *NF1* ablation is driven by Cre recombinase expressed under promoters active along the NC-SC differentiation axis. The ability to differentiate PNF-derived iPSCs toward NCs and SCs could complement the information coming from genetically modified mice.

In summary, we have generated *NF1*(−/−) iPSCs directly from PNFs. They represent an iPSC-based non-perishable cell model system for a benign tumor. *NF1*(−/−) iPSCs contain the same naturally occurring mutations as their primary counterparts and preserve their proliferative properties when differentiated from NCs toward SCs. SCs differentiated from PNF-derived iPSCs have a high tendency to form spheres. This cell-based model system constitutes a great tool to investigate the PNF cell of origin, the genetic and epigenetic changes required for progression toward MPNSTs and finally, a model to test new therapeutic strategies before pre-clinical *in vivo* models.

EXPERIMENTAL PROCEDURES

Patients, Plexiform Neurofibromas, and Tumor Processing

Tumor samples were kindly provided by NF1 patients after giving written informed consent for iPSC generation and genomic analysis studies. The study was approved by our Institutional Review Board and local ethical commitees. The patients were diagnosed according to standard diagnostic criteria (DeBella et al., 2000). Tumor specimens were obtained after surgery of five PNFs from five independent patients (two males, three females; ages 8–66 years). Immediately after excision, tumor samples were placed in DMEM medium (Gibco) containing 10% FBS (Gibco) + 1× Glx (Gibco) + 1× normocin antibiotic cocktail (InvivoGene), and shipped at room temperature to our laboratory. Tumors were processed as follows: surrounding fat tissue and skin were removed and tumors were cut into 1-mm pieces and cryopreserved in 10% DMSO (Sigma) + 90% FBS until used.

PNF-Derived SCs and Fibroblasts Cultures

PNF-derived SCs and fibroblasts were isolated as described previously (Serra et al., 2000). In brief, PNF pieces that were preserved in liquid nitrogen were thawed and digested with 160 U/mL collagenase type 1 and 0.8 U/mL dispase (Worthington, Lakewood, NJ) for 16 h at 37°C. Dissociated cells were washed and seeded onto 0.1 mg/mL poly-L-lysine (Sigma) and 4 μg/mL laminin (Gibco)-coated dishes in Schwann cell medium (SCM) and maintained at 37°C under a 10% CO_2 atmosphere. SCM is DMEM (Gibco) with 10% FBS, 500 U/mL penicillin/500 μg/mL streptomycin (Gibco), 0.5 mM 3-iso-butyl-1-methilxantine (Sigma), 2.5 mg/mL insulin (Sigma), 10 nM heregulin-β1 (PeproTech), and 0.5 μM forskolin (Sigma). One day after plating, culture medium was replaced by SCM without forskolin for an additional 2–3 days. This process was repeated in cycles and cells were passaged as needed with trypsin 0.05% (Gibco). SC purity was assessed by performing S100β staining as described previously (Serra et al., 2000). To isolate fibroblasts, dissociated cells were plated in DMEM 10% FBS media and passaged when necessary.

Reprogramming of SCs, Fibroblasts, and Digested Tumors

Between 1 × 10^4 and 2 × 10^4 cells were reprogrammed through the retroviral delivery of human cDNA coding for OCT4, SOX2, KLF4, and cMYC transcription factors as described previously (Raya et al., 2009). For non-integrative reprogramming, a Cytotune-iPS 2.0 Sendai Reprogramming Kit (Thermo Fisher Scientific) was used according to the manufacturer's protocol. Approximately 3 or 4 weeks after transduction, colonies displaying embryonic stem cell-like morphology and behavior were selected for further characterization and genotyping. iPSC established lines were grown on dishes coated with growth factor-reduced Matrigel (BD Biosciences) in mTESR1 medium (STEMCELL Technologies). See Supplemental Information for a detailed description of iPSC characterization.

Figure 5. *NF1*(−/−) Differentiating SCs Exhibited a Continuous High Proliferation Rate and a Lack of Myelinating Capacity

(A) Representative bright-field images after 20 days of differentiation from NC to SC for different *NF1* genotypes. 3PNFiPS(−/−) and 5PNFiPS(−/−) cells exhibited a high cell density and the formation of 3D spheres. Scale bars, 50 μm.

(B) Macroscopic detail of sphere formation in 3PNiPS(−/−) and 5PNFiPS(−/−) cells during SC differentiation.

(C) Proliferation capacity of differentiating SCs. Representative immunofluorescence images of Ki-67 (green) at 7 and 30 days of differentiation. DAPI was used to stain cell nuclei. Scale bars, 50 μm.

(D) Quantification of Ki-67-positive cells (percentage over total DAPI-positive nuclei) expressed as the mean ± SE (n = 3 independent differentiation experiments). At least 300 nuclei were counted per time point and sample. *p < 0.05, **p < 0.01, ***p < 0.001 (unpaired t test).

(E and F) Myelination capacity of control *NF1*(+/+) FiPS (E) and *NF1*(−/−) iPSCs (F). Myelination was assessed by co-culturing differentiated SCs (at 7 days) with rat DRG neurons for 30 days. SC myelination capacity was measured by immunostaining for TUJ1, S100b, and MPZ. Scale bars, 50 μm.

(G) PNF-derived SC immunostained with TUJ1, S100b, and MPZ. Scale bars, 50 μm.

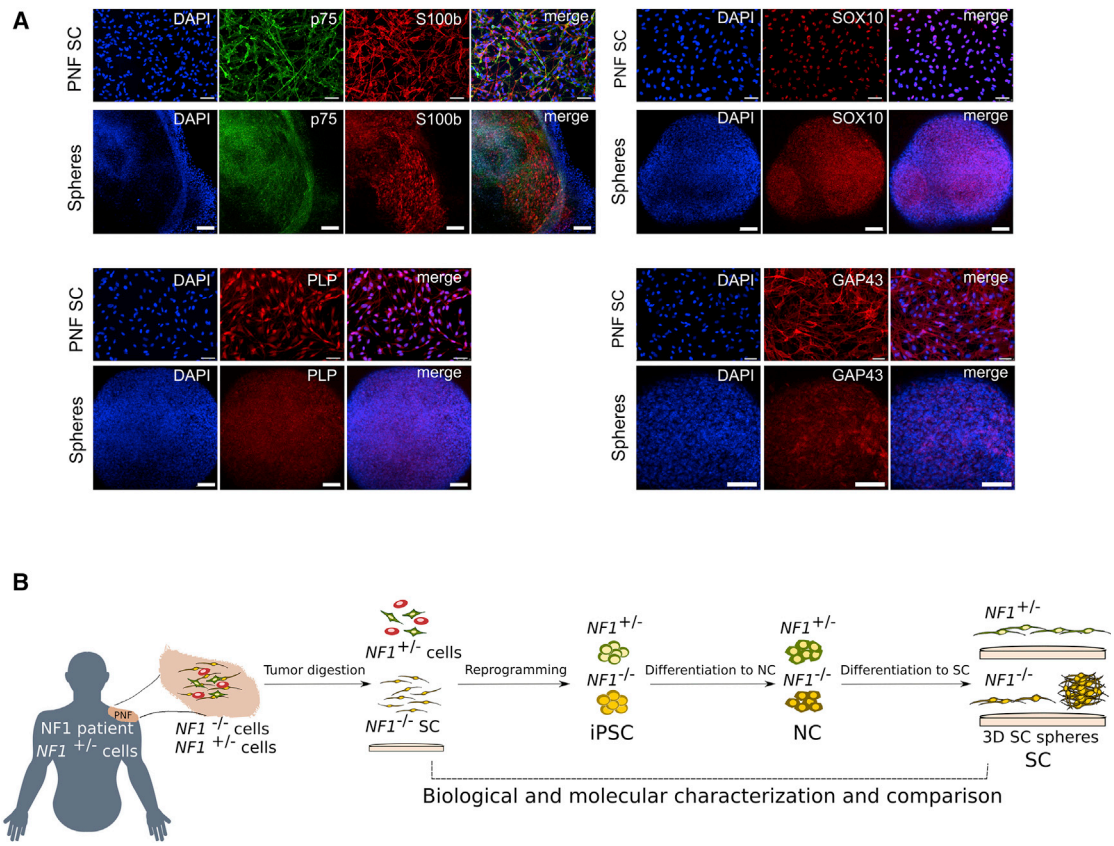

Figure 6. Sphere-Forming SCs from *NF1*(−/−) iPSCs Recapitulate the Expression Pattern of their PNF-Derived Primary SC Counterparts

(A) Representative immunofluorescence images showing expression of S100b, p75, SOX10, GAP43, and PLP, in 5PNF primary SCs (PNF SC) compared with sphere-forming 5PNFiPS(−/−) differentiating SCs, at 30 days of differentiation. Scale bars, 100 μm.

(B) Schematic representation of the generated PNF model.

Differentiation toward NCs and SCs

Neural crest differentiation was performed as described by Menendez et al. (2013) with some modifications. In brief, 9 × 10^4 cells/cm^2 were plated onto Matrigel-coated plates in mTESR medium. The following day, the medium was replaced with hESC maintenance medium: DMEM:F12 (Gibco) 1:1; 5 mg/mL BSA (Sigma); 500 U/mL penicillin/500 μg/mL streptomycin (Gibco); 2 mM GlutaMAX (Gibco); 1× MEM non-essential amino acids (Gibco); 1× trace elements A; 1× trace elements B; 1× trace elements C (Corning); 2-mercaptoethanol (Gibco); 10 μg/mL transferrin (Sigma); 50 μg/mL sodium L-ascorbate (Sigma); 10 ng/mL heregulin-β1 (PeproTech); 10 ng/mL activin A (PeproTech); 200 μg/mL LONG R3 IGFR (PeproTech); 8 ng/mL basic fibroblast growth factor 2 (PeproTech). Next day, the medium was replaced with neural crest induction/differentiation medium: hESC medium without activin and supplemented with 2 μM CHIR9902 (STEMCELL Technologies) and 20 μM SB432542 (STEMCELL Technologies), and was replaced every day. NCs were maintained in this medium and split with Accutase (Thermo Fischer Scientific) when necessary.

For SC differentiation NCs were plated onto 0.1 mg/mL poly-L-lysine (Sigma) and 4 μg/mL laminin (Gibco)-coated plates and cultured in SC differentiation medium: DMEM:F12 (3:1); 500 U/ml penicillin/500 μg/mL streptomycin antibiotics (Gibco); 5 μM forskolin (Sigma); 50 ng/mL heregulin-β1; 2% N2 supplement (Gibco); 1% FBS (Gibco). The medium was replaced twice a week.

Additional Experimental Procedures

Additional experimental procedures can be found in Supplemental Information.

REPOSITORIES

The iPSC lines generated have been banked banked and are currently distributed by the Spanish National Stem Cell Bank-Institute of Health Carlos III in compliance with the informed consent signed by the patient (see Table 1).

ACCESSION NUMBERS

Data are available at the Synapse repository with accession number syn17413894 (DOI: 10.7303/syn17413894.1) (https://www.synapse.org/#!Synapse:syn17413894/tables/).

SUPPLEMENTAL INFORMATION

Supplemental Information includes Supplemental Experimental Procedures, five figures, and five tables and can be found with this article online at https://doi.org/10.1016/j.stemcr.2019.01.001.

AUTHOR CONTRIBUTIONS

E.S. conceived the study. M.C., Y.R.-P., A.R., and E.S. designed the study and wrote the manuscript that was revised, corrected, and improved by all authors. M.C., H.M., and Y.R.-P. performed most of the experimental work. B.G. performed bioinformatic analysis. I.R. and E.C. performed NF1 genetic analysis. E.T., S.J.-D., J.B., and L.V. performed experimental work. I.B. and C.L. provided scientific input. M.C. and B.G. generated the figures for the paper. All authors approved the final version of the manuscript.

ACKNOWLEDGMENTS

This work has mainly been supported by an agreement from the Johns Hopkins University School of Medicine and the Neurofibromatosis Therapeutic Acceleration Program (NTAP). Its contents are solely the responsibility of the authors and do not necessarily represent the official views of the Johns Hopkins University School of Medicine. The work has also been partially supported by the Spanish Ministry of Science and Innovation, Carlos III Health Institute (ISCIII) (PI14/00577; PI17/00524; RD16/0011/0024; and PIE14/00061) Plan Estatal de I. D. i 2013–16; co-financed by the FEDER program; and by the Government of Catalonia (2017-SGR-899) and CERCA Program/Generalitat de Catalunya. We thank the patients and their physicians who contributed the original samples. We would like to specially thank the Asociación de Afectados de Neurofibromatosis for their constant support and coordination with patients. We also give thanks for the support of ACNefi and the Spanish Association Against Cancer (AECC) for recognizing our group with one of its awards. We thank the IGTP core facilities and their staff for their contribution and technical support: Translational Genomics Core Facility; High Content Genomics and Bioinformatics Core Facility; Flow Cytometry (Gerard Requena and Marco A. Fernández); Microscopy Core facility (Gerard Requena). We also thank the National Center for Genomic Analysis (CNAG). Finally, we would like to thank Dr. Jaishri Blakeley, Dr. Sharad Verma, and people at NTAP for their constant support and appreciate insightful discussions of the different PIs funded by the NTAP Cell Culture Initiative.

Received: June 11, 2018
Revised: December 31, 2018
Accepted: January 1, 2019
Published: January 31, 2019

REFERENCES

Anastasaki, C., Woo, A.S., Messiaen, L.M., and Gutmann, D.H. (2015). Elucidating the impact of neurofibromatosis-1 germline mutations on neurofibromin function and dopamine-based learning. Hum. Mol. Genet. *24*, 3518–3528.

Ban, H., Nishishita, N., Fusaki, N., Tabata, T., Saeki, K., Shikamura, M., Takada, N., Inoue, M., Hasegawa, M., Kawamata, S., and Nishikawa, S. (2011). Efficient generation of transgene-free human induced pluripotent stem cells (iPSCs) by temperature-sensitive Sendai virus vectors. Proc. Natl. Acad. Sci. U S A *108*, 14234–14239.

Beert, E., Brems, H., Daniels, B., De Wever, I., Van Calenbergh, F., Schoenaers, J., Debiec-Rychter, M., Gevaert, O., De Raedt, T., Van Den Bruel, A., et al. (2011). Atypical neurofibromas in neurofibromatosis type 1 are premalignant tumors. Genes Chromosomes Cancer *50*, 1021–1032.

Bernhardt, M., Novak, D., Assenov, Y., Orouji, E., Knappe, N., Weina, K., Reith, M., Larribere, L., Gebhardt, C., Plass, C., et al. (2017). Melanoma-derived iPCCs show differential tumorigenicity and therapy response. Stem Cell Rep. *8*, 1379–1391.

Buchstaller, J., Clapp, D.W., Parada, L.F., and Zhu, Y. (2012). Cell of origin and the contribution of microenvironment in NF1 tumorigenesis and therapeutic implications. In Neurofibromatosis Type 1:Molecular and Cellular Biology, M. Upadhyaya and D.N. Cooper, eds. (Springer Berlin Heidelberg), pp. 549–568.

Carrió, M., Gel, B., Terribas, E., Carolina Zucchiatti, A., Moliné, M., Rosas, I., Teulé, A., Ramón y Cajal, S., López-Gutiérrez, J.C., Blanco, I., et al. (2018). Analysis of intra-tumor heterogeneity in neurofibromatosis type 1 plexiform neurofibromas and neurofibromas with atypical features: correlating histological and genomic findings. Hum. Mutat. *39*, 1112–1125.

Castellanos, E., Gel, B., Rosas, I., Tornero, E., Santín, S., Pluvinet, R., Velasco, J., Sumoy, L., Del Valle, J., Perucho, M., et al. (2017). A comprehensive custom panel design for routine hereditary cancer testing: preserving control, improving diagnostics and revealing a complex variation landscape. Sci. Rep. *7*, 39348.

Chen, Z., Liu, C., Patel, A.J., Liao, C.-P., Wang, Y., and Le, L.Q. (2014). Cells of origin in the embryonic nerve roots for NF1-associated plexiform neurofibroma. Cancer Cell *26*, 695–706.

Däschner, K., Assum, G., Eisenbarth, I., Krone, W., Hoffmeyer, S., Wortmann, S., Heymer, B., and Kehrer-Sawatzki, H. (1997). Clonal origin of tumor cells in a plexiform neurofibroma with LOH in NF1 intron 38 and in dermal neurofibromas without LOH of the NF1 gene. Biochem. Biophys. Res. Commun. *234*, 346–350.

DeBella, K., Szudek, J., and Friedman, J.M. (2000). Use of the National Institutes of Health criteria for diagnosis of neurofibromatosis 1 in children. Pediatrics *105* (3 Pt 1), 608–614.

Dombi, E., Baldwin, A., Marcus, L.J., Fisher, M.J., Weiss, B., Kim, A., Whitcomb, P., Martin, S., Aschbacher-Smith, L.E., Rizvi, T.A., et al. (2016). Activity of selumetinib in neurofibromatosis type 1-related plexiform neurofibromas. N. Engl. J. Med. *375*, 2550–2560.

Ebrahimi, B. (2015). Reprogramming barriers and enhancers: strategies to enhance the efficiency and kinetics of induced pluripotency. Cell Regen. (Lond) *4*, 10.

Ferner, R.E. (2007). Neurofibromatosis 1 and neurofibromatosis 2: a twenty-first century perspective. Lancet Neurol. *6*, 340–351.

Garcia-Linares, C., Fernández-Rodríguez, J., Terribas, E., Mercadé, J., Pros, E., Benito, L., Benavente, Y., Capellà, G., Ravella, A., Blanco, I., et al. (2011). Dissecting loss of heterozygosity (LOH) in neurofibromatosis type 1-associated neurofibromas: importance of copy neutral LOH. Hum. Mutat. *32*, 78–90.

Gosline, S.J.C., Weinberg, H., Knight, P., Yu, T., Guo, X., Prasad, N., Jones, A., Shrestha, S., Boone, B., Levy, S.E., et al. (2017). A high-throughput molecular data resource for cutaneous neurofibromas. Sci. Data *4*, 170045.

Higham, C.S., Dombi, E., Rogiers, A., Bhaumik, S., Pans, S., Connor, S.E.J., Miettinen, M., Sciot, R., Tirabosco, R., Brems, H., et al. (2018). The characteristics of 76 atypical neurofibromas as precursors to neurofibromatosis 1 associated malignant peripheral nerve sheath tumors. Neuro. Oncol. *20*, 818–825.

Hirbe, A.C., Dahiya, S., Miller, C.A., Li, T., Fulton, R.S., Zhang, X., McDonald, S., DeSchryver, K., Duncavage, E.J., Walrath, J., et al. (2015). Whole exome sequencing reveals the order of genetic changes during malignant transformation and metastasis in a single patient with NF1-plexiform neurofibroma. Clin. Cancer Res. *21*, 4201–4211.

Jessen, K.R., and Mirsky, R. (2005). The origin and development of glial cells in peripheral nerves. Nat. Rev. Neurosci. *6*, 671–682.

Kim, H.A., Ling, B., and Ratner, N. (1997). *Nf1*-deficient mouse Schwann cells are angiogenic and invasive and can be induced to hyperproliferate: reversion of some phenotypes by an inhibitor of farnesyl protein transferase. Mol. Cell. Biol. *17*, 862–872.

Kim, H.A., Rosenbaum, T., Marchionni, M.A., Ratner, N., and DeClue, J.E. (1995). Schwann cells from neurofibromin deficient mice exhibit activation of p21ras, inhibition of cell proliferation and morphological changes. Oncogene *11*, 325–335.

Kim, J., Hoffman, J.P., Alpaugh, R.K., Rhim, A.D., Reichert, M., Stanger, B.Z., Furth, E.E., Sepulveda, A.R., Yuan, C.-X., Won, K.-J., et al. (2013). An iPSC line from human pancreatic ductal adenocarcinoma undergoes early to invasive stages of pancreatic cancer progression. Cell Rep. *3*, 2088–2099.

Kim, J., and Zaret, K.S. (2015). Reprogramming of human cancer cells to pluripotency for models of cancer progression. EMBO J. *34*, 739–747.

Kluwe, L., Friedrich, R.E., and Mautner, V.F. (1999). Allelic loss of the NF1 gene in NF1-associated plexiform neurofibromas. Cancer Genet. Cytogenet. *113*, 65–69.

Kotini, A.G., Chang, C.-J., Chow, A., Yuan, H., Ho, T.-C., Wang, T., Vora, S., Solovyov, A., Husser, C., Olszewska, M., et al. (2017). Stage-specific human induced pluripotent stem cells map the progression of myeloid transformation to transplantable leukemia. Cell Stem Cell *20*, 315–328.e7.

Kraniak, J.M., Chalasani, A., Wallace, M.R., and Mattingly, R.R. (2018). Development of 3D culture models of plexiform neurofibroma and initial application for phenotypic characterization and drug screening. Exp. Neurol. *299*, 289–298.

Krone, W., Jirikowski, G., Mühleck, O., Kling, H., and Gall, H. (1983). Cell culture studies on neurofibromatosis (von Recklinghausen). II. Occurrence of glial cells in primary cultures of peripheral neurofibromas. Hum. Genet. *63*, 247–251.

Larribere, L., Wu, H., Novak, D., Galach, M., Bernhardt, M., Orouji, E., Weina, K., Knappe, N., Sachpekidis, C., Umansky, L., et al. (2015). NF1 loss induces senescence during human melanocyte differentiation in an iPSC-based model. Pigment Cell Melanoma Res. *28*, 407–416.

Lee, G., Kim, H., Elkabetz, Y., Al Shamy, G., Panagiotakos, G., Barberi, T., Tabar, V., and Studer, L. (2007). Isolation and directed differentiation of neural crest stem cells derived from human embryonic stem cells. Nat. Biotechnol. *25*, 1468–1475.

Lee, G., Chambers, S.M., Tomishima, M.J., and Studer, L. (2010). Derivation of neural crest cells from human pluripotent stem cells. Nat. Protoc. *5*, 688–701.

Li, H., Chang, L.-J., Neubauer, D.R., Muir, D.F., and Wallace, M.R. (2016). Immortalization of human normal and NF1 neurofibroma Schwann cells. Lab. Invest. *96*, 1105–1115.

Maertens, O., Brems, H., Vandesompele, J., De Raedt, T., Heyns, I., Rosenbaum, T., De Schepper, S., De Paepe, A., Mortier, G., Janssens, S., et al. (2006). Comprehensive NF1 screening on cultured Schwann cells from neurofibromas. Hum. Mutat. *27*, 1030–1040.

Mautner, V.-F., Asuagbor, F.A., Dombi, E., Funsterer, C., Kluwe, L., Wenzel, R., Widemann, B.C., and Friedman, J.M. (2008). Assessment of benign tumor burden by whole-body MRI in patients with neurofibromatosis 1. Neuro. Oncol. *10*, 593–598.

McCarron, K.F., and Goldblum, J.R. (1998). Plexiform neurofibroma with and without associated malignant peripheral nerve sheath tumor: a clinicopathologic and immunohistochemical analysis of 54 cases. Mod. Pathol. *11*, 612–617.

Menendez, L., Kulik, M.J., Page, A.T., Park, S.S., Lauderdale, J.D., Cunningham, M.L., and Dalton, S. (2013). Directed differentiation of human pluripotent cells to neural crest stem cells. Nat. Protoc. *8*, 203–212.

Miller, S.J., Jessen, W.J., Mehta, J., Hardiman, A., Sites, E., Kaiser, S., Jegga, A.G., Li, H., Upadhyaya, M., Giovannini, M., et al. (2009). Integrative genomic analyses of neurofibromatosis tumours identify SOX9 as a biomarker and survival gene. EMBO Mol. Med. *1*, 236–248.

Muir, D., Neubauer, D., Lim, I.T., Yachnis, A.T., and Wallace, M.R. (2001). Tumorigenic properties of neurofibromin-deficient neurofibroma Schwann cells. Am. J. Pathol. *158*, 501–513.

Packer, R.J., and Rosser, T. (2002). Therapy for plexiform neurofibromas in children with neurofibromatosis 1: an overview. J. Child Neurol. *17*, 638–641.

Pan, X.-Y., Tsai, M.-H., Wuputra, K., Ku, C.-C., Lin, W.-H., Lin, Y.-C., Kishikawa, S., Noguchi, M., Saito, S., Lin, C.-S., and Yokoyama, K.K. (2017). Application of cancer cell reprogramming technology to human cancer research. Anticancer Res. *37*, 3367–3377.

Papapetrou, E.P. (2016). Patient-derived induced pluripotent stem cells in cancer research and precision oncology. Nat. Med. *22*, 1392–1401.

Peltonen, J., Jaakkola, S., Lebwohl, M., Renvall, S., Risteli, L., Virtanen, I., and Uitto, J. (1988). Cellular differentiation and expression of matrix genes in type 1 neurofibromatosis. Lab. Invest. *59*, 760–771.

Pemov, A., Li, H., Patidar, R., Hansen, N.F., Sindiri, S., Hartley, S.W., Wei, J.S., Elkahloun, A., Chandrasekharappa, S.C., Boland, J.F., et al. (2017). The primacy of NF1 loss as the driver of tumorigenesis in neurofibromatosis type 1-associated plexiform neurofibromas. Oncogene *36*, 3168–3177.

Prada, C.E., Rangwala, F.A., Martin, L.J., Lovell, A.M., Saal, H.M., Schorry, E.K., and Hopkin, R.J. (2012). Pediatric plexiform neurofibromas: impact on morbidity and mortality in neurofibromatosis type 1. J. Pediatr. *160*, 461–467.

Rasmussen, S.A., Overman, J., Thomson, S.A., Colman, S.D., Abernathy, C.R., Trimpert, R.E., Moose, R., Virdi, G., Roux, K., Bauer, M., et al. (2000). Chromosome 17 loss-of-heterozygosity studies in benign and malignant tumors in neurofibromatosis type 1. Genes. Chromosomes Cancer *28*, 425–431.

Ratner, N., and Miller, S.J. (2015). A RASopathy gene commonly mutated in cancer: the neurofibromatosis type 1 tumour suppressor. Nat. Rev. Cancer *15*, 290–301.

Raya, Á., Rodríguez-Pizà, I., Guenechea, G., Vassena, R., Navarro, S., Barrero, M.J., Consiglio, A., Castellà, M., Río, P., Sleep, E., et al. (2009). Disease-corrected haematopoietic progenitors from Fanconi anaemia induced pluripotent stem cells. Nature *460*, 53–59.

Reiprich, S., Kriesch, J., Schreiner, S., and Wegner, M. (2010). Activation of Krox20 gene expression by Sox10 in myelinating Schwann cells. J. Neurochem. *112*, 744–754.

Rosenbaum, T., Boissy, Y.L., Kombrinck, K., Brannan, C.I., Jenkins, N.A., Copeland, N.G., and Ratner, N. (1995). Neurofibromin-deficient fibroblasts fail to form perineurium in vitro. Development *121*, 3583–3592.

Serra, E., Rosenbaum, T., Winner, U., Aledo, R., Ars, E., Estivill, X., Lenard, H.G., and Lázaro, C. (2000). Schwann cells harbor the somatic NF1 mutation in neurofibromas: evidence of two different Schwann cell subpopulations. Hum. Mol. Genet. *9*, 3055–3064.

Serra, E., Rosenbaum, T., Nadal, M., Winner, U., Ars, E., Estivill, X., and Lázaro, C. (2001). Mitotic recombination effects homozygosity for NF1 germline mutations in neurofibromas. Nat. Genet. *28*, 294–296.

Steinmann, K., Kluwe, L., Friedrich, R.E., Mautner, V.-F., Cooper, D.N., and Kehrer-Sawatzki, H. (2009). Mechanisms of loss of heterozygosity in neurofibromatosis type 1-associated plexiform neurofibromas. J. Invest. Dermatol. *129*, 615–621.

Takahashi, K., and Yamanaka, S. (2006). Induction of pluripotent stem cells from mouse embryonic and adult fibroblast cultures by defined factors. Cell *126*, 663–676.

VM, and Riccardi. (1992). Neurofibromatosis: Phenotype, Natural History, and Pathogenesis, Second Edition (Johns Hopkins University Press).

Wallace, M.R., Rasmussen, S.A., Lim, I.T., Gray, B.A., Zori, R.T., and Muir, D. (2000). Culture of cytogenetically abnormal Schwann cells from benign and malignant NF1 tumors. Genes. Chromosomes Cancer *27*, 117–123.

Wegscheid, M.L., Anastasaki, C., and Gutmann, D.H. (2018). Human stem cell modeling in neurofibromatosis type 1 (NF1). Exp. Neurol. *299*, 270–280.

Stem Cell Reports, Volume *12*

Supplemental Information

Reprogramming Captures the Genetic and Tumorigenic Properties of Neurofibromatosis Type 1 Plexiform Neurofibromas

Meritxell Carrió, Helena Mazuelas, Yvonne Richaud-Patin, Bernat Gel, Ernest Terribas, Imma Rosas, Senda Jimenez-Delgado, Josep Biayna, Leen Vendredy, Ignacio Blanco, Elisabeth Castellanos, Conxi Lázaro, Ángel Raya, and Eduard Serra

FIGURE S1

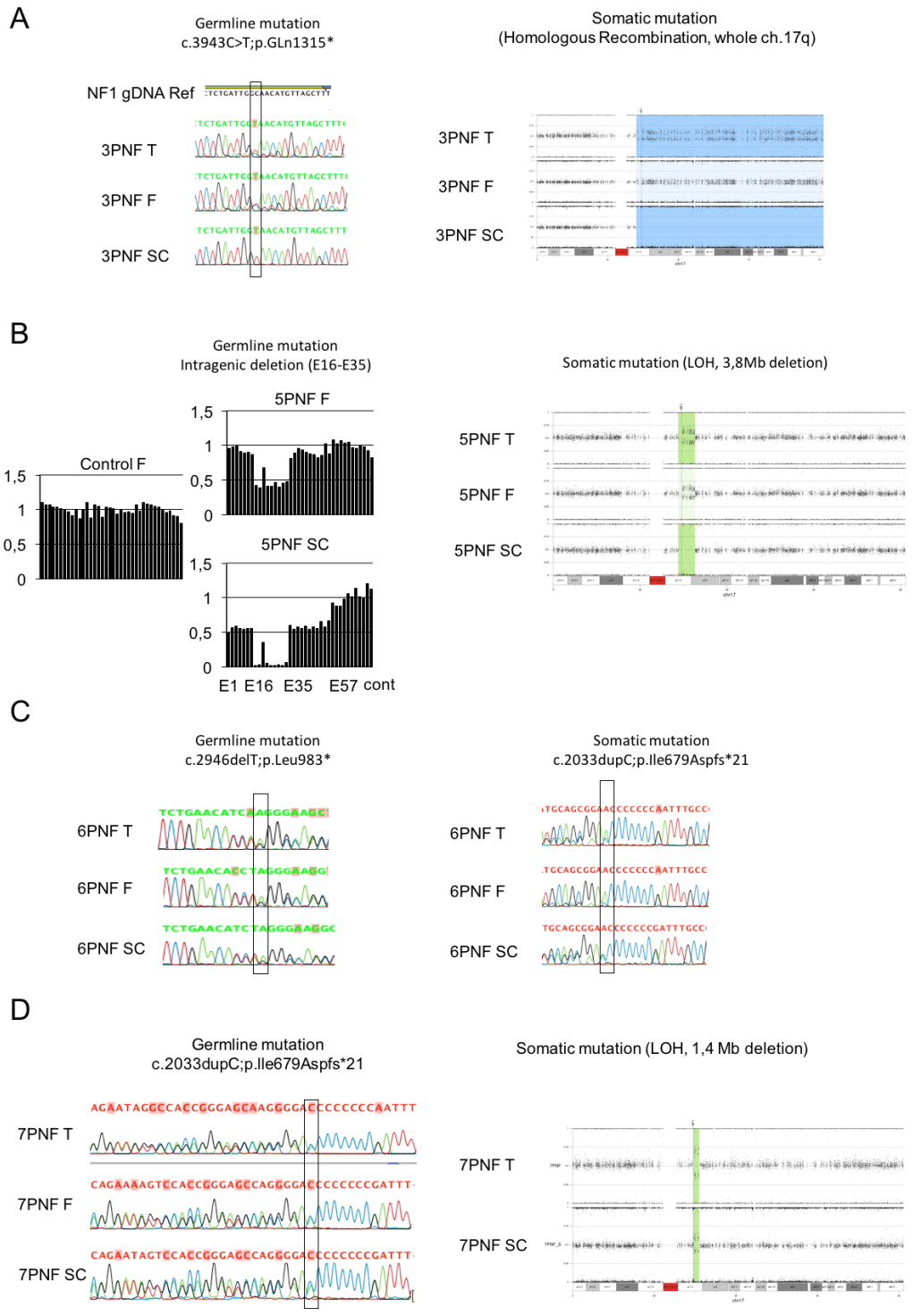
A
Germline mutation
c.3943C>T;p.GLn1315*
NF1 gDNA Ref
3PNF T
3PNF F
3PNF SC
Somatic mutation
(Homologous Recombination, whole ch.17q)
3PNF T
3PNF F
3PNF SC
B
Germline mutation
Intragenic deletion (E16-E35)
Control F
5PNF F
5PNF SC
1,5
1
0,5
0
E1 E16 E35 E57 cont
Somatic mutation (LOH, 3,8Mb deletion)
5PNF T
5PNF F
5PNF SC
C
Germline mutation
c.2946delT;p.Leu983*
6PNF T
6PNF F
6PNF SC
Somatic mutation
c.2033dupC;p.Ile679Aspfs*21
6PNF T
6PNF F
6PNF SC
D
Germline mutation
c.2033dupC;p.Ile679Aspfs*21
7PNF T
7PNF F
7PNF SC
Somatic mutation (LOH, 1,4 Mb deletion)
7PNF T
7PNF SC

Figure S1. *NF1* germline and somatic mutation analysis in the four PNFs used to generate the banked iPSC lines.

A) 3PNF *NF1* mutational analysis. Left: Sanger sequencing showing the germline mutation c.3943C>T;p.GLn1315* in the *NF1* gene. The germline mutation is present in the tumor (3PNF T), in tumor fibroblasts (3PNF F) and in tumor SC (3PNF SC). Right: B-allele frequency (BAF) data (a detailed view from chromosome 17) from SNP-array analysis showing the somatic mutation of 3PNF. Somatic *NF1* inactivation is produced by mitotic recombination generating CN-LOH in 17q and the reduction to homozygosity for the constitutional *NF1* mutation. LOH is observed in 3PNF and in 100% of cells in 3PNF SC. Fibroblast culture (3PNF F) is an early passage and still exhibit a residual LOH due to the presence of tumor SCs.
B) 5PNF *NF1* mutational analysis. Left: MLPA analysis showing an intragenic deletion in the *NF1* gene, from exon 16 (E16) to exon 57 (E57). The deletion is detected in tumor fibroblasts (5PNF F) and in tumor SC (5PNF SC). Right: detailed view of BAF for chromosome 17. Somatic *NF1* inactivation is produced by a deletion generating CN-LOH in 17q and the reduction to homozygosity for the constitutional *NF1* mutation. LOH is observed in 5PNF and in 100% of cells in 5PNF SC.
C) 6PNF *NF1* mutational analysis. Left: Sanger sequencing showing the germline mutation c.2946delT;p.Leu983* present in the tumor (6PNF T), tumor fibroblasts (6PNF F) and tumor SCs (6PNF SC). Right: sanger sequencing showing the somatic mutation c.2033dupC;p.ile679Aspf*21 only present 6PNF SC and not in 6PNF F.
D) 7PNF *NF1* mutational analysis. Left: Sanger sequencing showing the germline mutation c.2033dupC;p.ile679Aspf*21 present in the tumor (7PNF T), tumor fibroblasts (7PNF F) and tumor SC (7 PNF SC). Right: detailed view of BAF for chromosome 17. Somatic *NF1* inactivation is produced by a deletion generating CN-LOH in 17q. LOH is observed in 7PNF and in 7PNF SC.

FIGURE S2

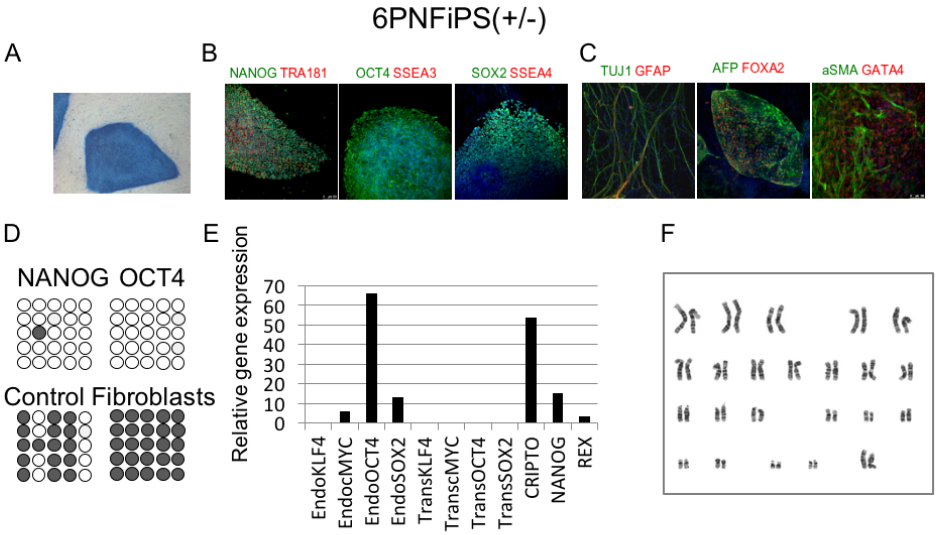

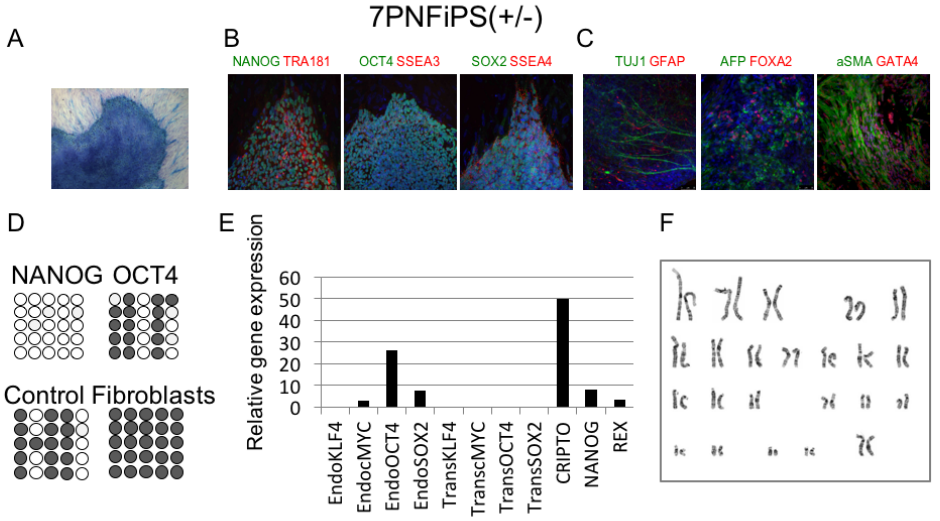

G

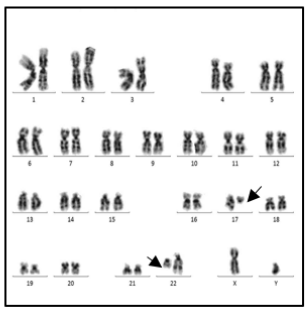

5PNF SC passage 3
46,XY,t(17;22)(q10;q13.3)

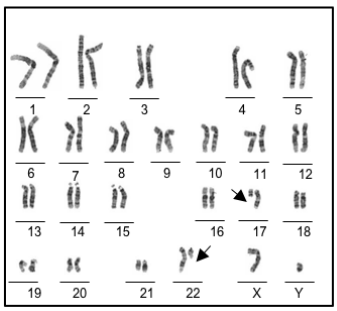

5PNFiPS (NF1-/-) passage 20
46,XY,t(17;22)(q10;q13.3)

Figure S2. iPSC Characterization of the additional banked NF1 iPSCs lines.

A) Morphology and alkaline phosphatase staining of a representative colony. Scale bar: 100µm
B) Pluripotency markers. Scale bar: 100µm
C) *In vitro* differentiation potential. Scale bar: 100µm
D) Bisulphite sequencing showing demethylation of the *NANOG and POU5F1(*OCT4*)* promoters.
E) RT-qPCR analysis characterizing the expression levels of reprogramming genes either endogenous. (iPSC) or retroviral-derived (transgenes). Expression of pluripotency markers (CRIPTO, NANOG, REX) are also shown.
F) karyotypes at passage 20.
G) Karyotype of the 5PNF-derived SCs (5PNF SC) showing the presence of the same translocation t(17;22) as in the 5PNFiPS N(-/-) cell line that causes the somatic *NF1* mutation.

FIGURE S3

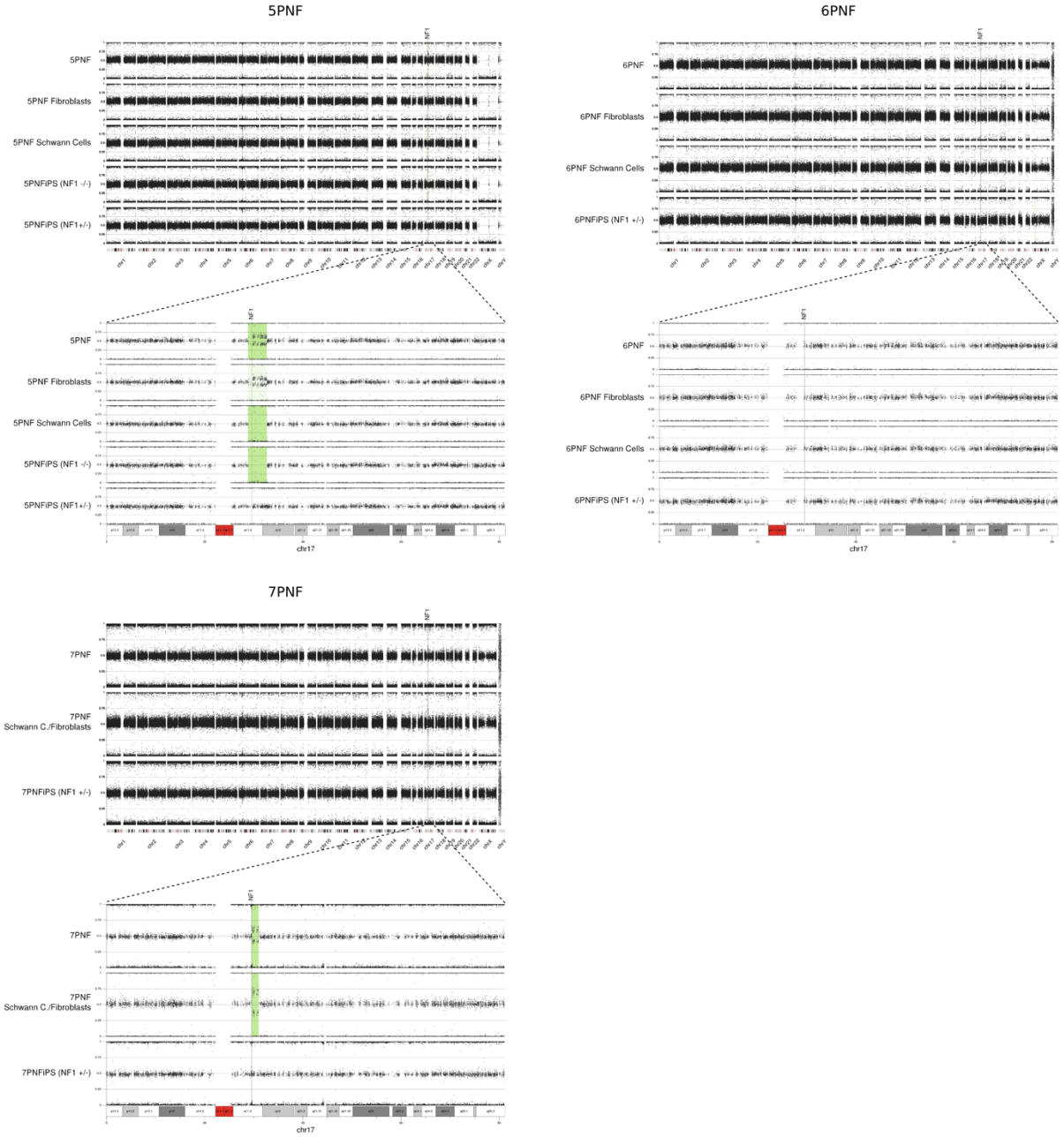

Figure S3. Genomic characterization of tumors, tumor isolated cells and corresponding iPSC lines.

B-allele frequency (BAF) data along the genome is plotted for all samples associated to each PNF. Green shaded regions denote somatic LOH due to genomic loss. Fibroblast cultures from tumor 5PNF are early passages in which LOH can still be detected due to the presence of *NF1*(-/-) Schwann cells. 7PNF Schwann cells/Fibroblasts is a heterogeneous cell culture (60% SC and 40% fibroblasts). The position of *NF1* is marked with a vertical black line.

FIGURE S4

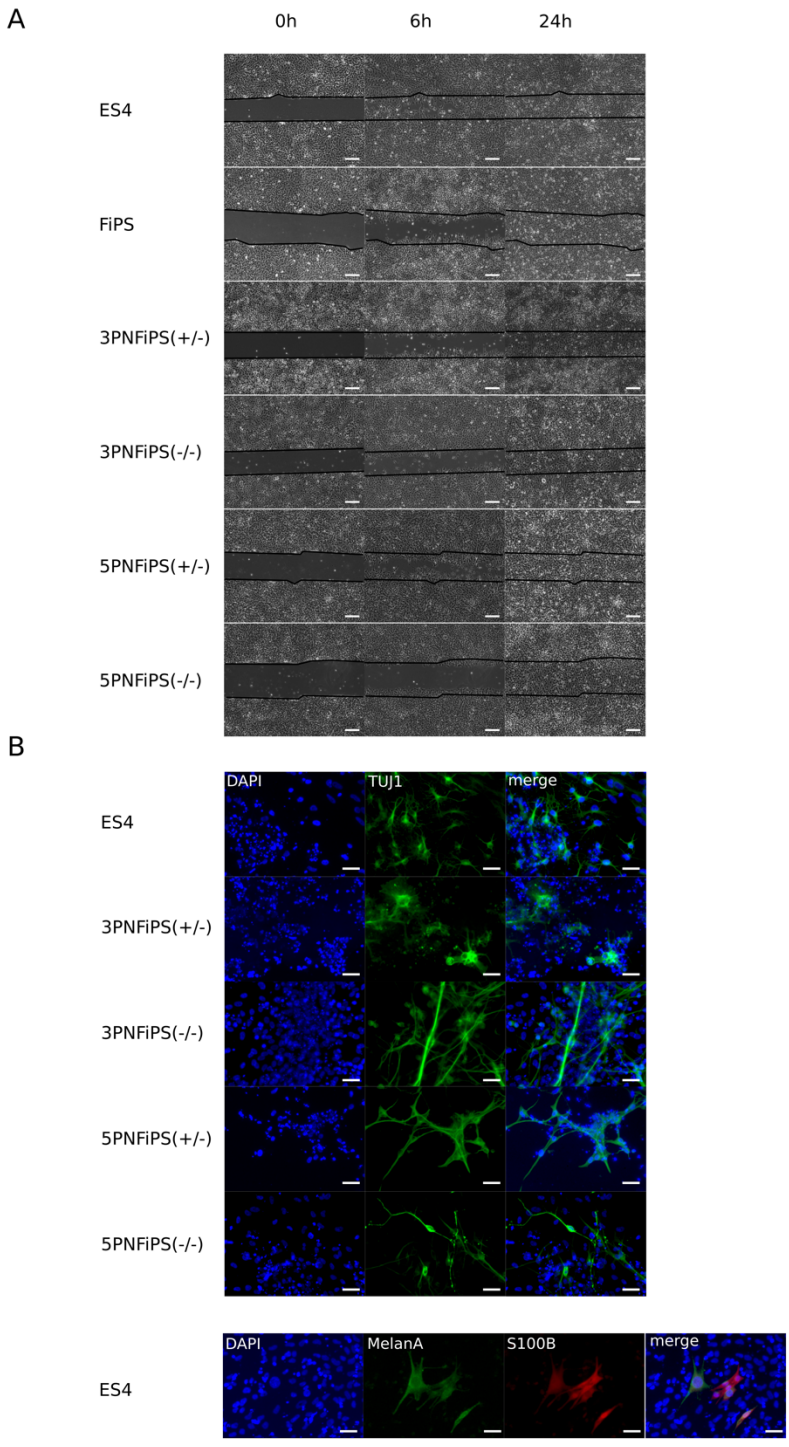

Figure S4. iPSC-derived NCSC lines have the capacity to migrate and differentiate into different NC-derivatives.

A) Scratch assay. A cell free-free gap was created using a pipette tip and migration capacity was measured by taking images of the same region at 6 and 24 hours after gap creation. Scale bar= 150µM. **B)** Differentiation capacity of generated NC towards peripheral neurons (Tuj1+) and melanocytes (MelanA+ and S100B+). Scale bar= 50µM.

FIGURE S5

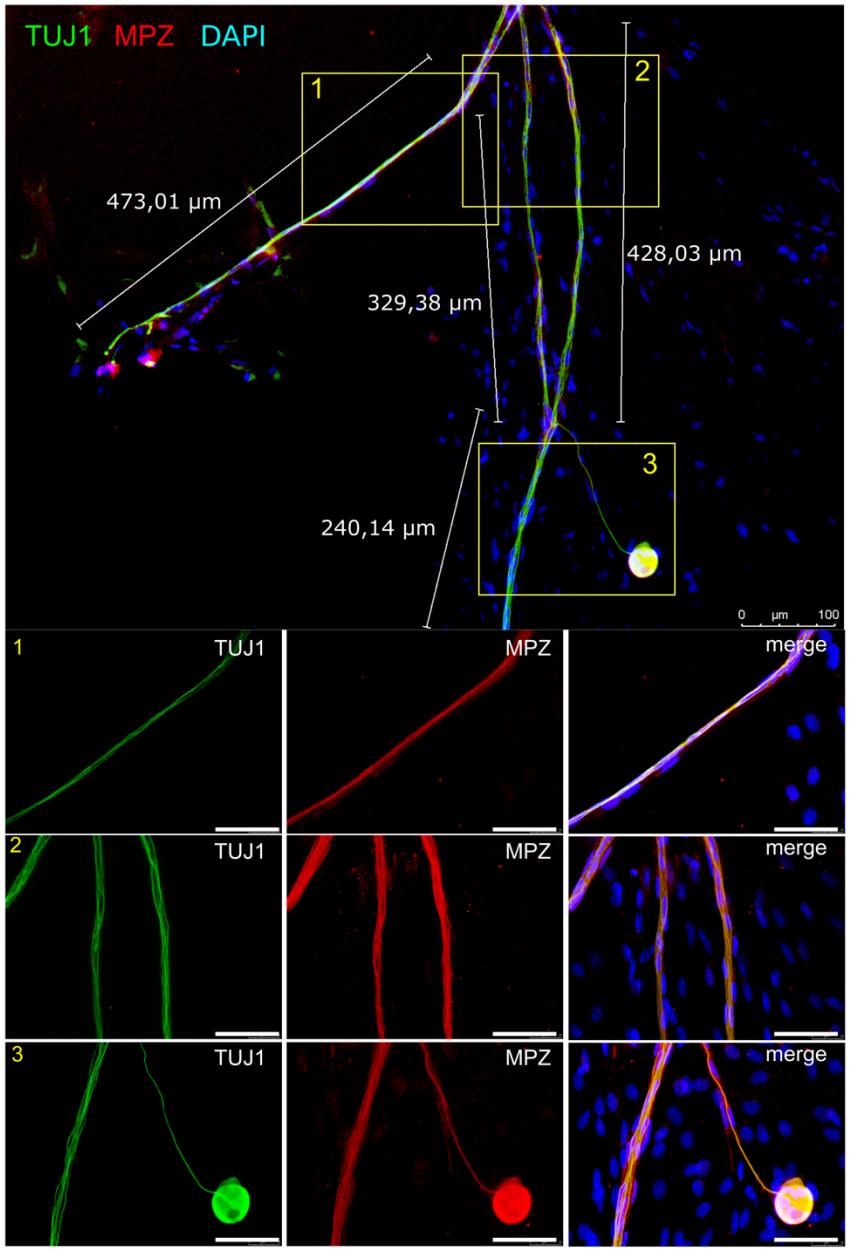

FIGURE S5. Myelin quantification of FiPS-differentiated SC.

The myelination capacity of FiPS-differentiated SCs was assessed by co-culturing cells at 7 days of differentiation with rat DRG neurons for 30 days. SC specification and myelination was measured by immunostaining for TUJ1 (green) andMPZ (red). The length of myelinated axons was measured using LEICA LASAF software and are marked by a white line. Scale bar: 50µm.

TABLE S1. Reprogramming information

TUMOR INFORMATION	REPROGRAMMING INFORMATION						
Tumor ID	Method	Reprogrammed cell	Num. of clones	NF1 mutation			iPSC LINE BANKING NAME
				Germline	Somatic		
					yes	No	
3PNF	Rv	PNF skin fibroblasts*	7	7	7*		
		PNF Schwann cells	10	10	10		
	Sv	PNF skin fibroblasts*	9	9		2	3PNFiPS(+/-) 3PNF_FiPSsv_PM
					7*		
		PNF Schwann cells	12	12	12		3PNFiPS(-/-) 3PNF_SiPSsv_MM
5PNF	Rv	PNF endoneurial fibroblasts	0				
		PNF Schwann cells	2	2	2		5PNFiPS(-/-)_Rv
	Sv	Digested PNF	12	12		1	5PNFiPS(+/-) 5PNF_TDiPSsv_PM
					11		5PNFiPS(-/-) 5PNF_TDiPSsv_MM
6PNF	Rv	PNF endoneurial fibroblasts	1	1	0	1	6PNFiPS(+/-)_Rv
		PNF Schwann cells	10	10	0	10	6PNFiPS(+/-) 6PNF_SiPSrv_PM
	Sv	Digested PNF	10	10	0	10	
7PNF	Rv	PNF endoneurial fibroblasts	1	1	0	1	
		Mix population T(40% PNF Schwann cell, 60% endoneurial fibroblasts)	12	12	0	12	7PNFiPS(+/-) 7PNF_TDiPSrv_PM
13PNF	Sv	PNF endoneurial fibroblasts	11	11	0	11	13PNFiPS(+/-)
		PNF Schwann cells	40	40	0	40	13PNFiPS(+/-)
		Digested PNF	27	27	0	27	

*The skin used was covering the PNF. When skin was separated, part of the tumor was still left.

TABLE S2. Sample authentication.

AmpFISTR Identifiler loci	3PNF	5PNF	6PNF	7PNF
CSF1PO	11,14	10	10,12	11,13
D2S1338	17,24	17,19	17,23	24
D3S1358	15,16	15,16	16,18	15,17
D5S818	10,11	12,13	11,13	10,12
D7S820	10	10,13	11	8,12
D8S1179	10,14	8,13	10,12	13,14
D13S317	8,13	8,12	11,14	8,13
D16S539	9,12	12,13	9,13	11,12
D18S51	13,15	15,16	11,13	12,15
D19S433	12,14.2	14,15	13,14	13,15
D21S11	30,32.2	29	29,30.2	29,30
FGA	21,24	21,23	21,27	20,25
THO1	8,9.3	9,3	7,9.3	6,9.3
TPOX	8	10,11	9,11	10,11

TABLE S3. List of somatic mutations.
The list includes all somatic mutations identified in each sample, meeting the following criteria: exonic or present in canonical splice sites, passing manual validation and excluding synonymous mutations. The list includes only non-*NF1* mutations.
See attached Supplemental_Table_S3.xls

TABLE S4. Primers for RT-qPCR.

Gene	Sequence(5′-3′)		UPL
POU5F1	*Forward*	cttcgcaagccctcatttc	60
	Reverse	gagaaggcgaaatccgaag	
POU3F1	*Forward*	ttctcaagtgccccaagc	78
	Reverse	ccggttgcagaaccagac	
NGFR	*Forward*	ccttccacgctgtctcca	60
	Reverse	cctaggcaagcatcccatc	
SOX10	*Forward*	gacacggttttccacttccta	25
	Reverse	gtcctcgcaaagagtccaac	
TFAP2A	*Forward*	ggtgaaccccaacgaagtc	73
	Reverse	accgtgaccttgtacttcgag	
S100B	*Forward*	ggaaggggtgagacaagga	73
	Reverse	ggtggaaaacgtcgatgag	
CDH19	*Forward*	tgtaccagaggaaatgaatacgac	78
	Reverse	catatatgtcacctgttctttcatca	
ITGA4	*Forward*	atgcaggatcggaaagaatc	78
	Reverse	ccacaaggttctccattaggg	
PLP1	*Forward*	cttcaacacctggaccacct	60
	Reverse	ccatgggagaacaccataca	
GAP43	*Forward*	gctccaagcctgatgagc	12
	Reverse	gctctgtggcagcatcac	
EGR2	*Forward*	gctgctacccagaaggcata	60
	Reverse	ggatgaggctgtggttgaa	
PMP22	*Forward*	ctgtcgatcatcttcagcattc	29
	Reverse	agcactcatcacgcacagac	
MPZ	*Forward*	ttcccatctcctgcatcc	55
	Reverse	ctgggccacctggtagag	
EndoKLF4	*Forward*	agcctaaatgatggtgcttggt	68
	Reverse	ttgaaaactttggcttccttgtt	
EndoMYC	*Forward*	cgggcgggcactttg	55
	Reverse	ggagagtcgcgtccttgct	
EndoOCT4	*Forward*	gggtttttgggattaagttcttca	63
	Reverse	gcccccacccttttgtgtt	
EndoSOX2	*Forward*	caaaaatggccatgcaggtt	63
	Reverse	agttgggatcgaacaaaagctatt	
TransKLF4	*Forward*	tggactacaaggacgacgatga	60
	Reverse	cgtcgctgacagccatga	
TransMYC	*Forward*	tggactacaaggacgacgatga	77
	Reverse	gttcctgttggtgaagctaacgt	
TransOCT4	*Forward*	tggactacaaggacgacgatga	58
	Reverse	caggtgtcccgccatga	
TransSOX2	*Forward*	gctcgaggttaacgaattcatgt	57
	Reverse	gcccggcggcttca	
CRIPTO	*Forward*	cggaactgtgagcacgatgt	66
	Reverse	gggcagccaggtgtcatg	
NANOG	*Forward*	acaactggccgaagaatagca	63
	Reverse	ggttcccagtcgggttcac	
REX	*Forward*	cctgcaggcggaaatagaac	61
	Reverse	gcacacatagccatcacataagg	

TABLE S5. Antibody list.

Antibody	Supplier	Reference	Dilution
Rabbit anti-NF1	Bethyl laboratories	A300-140A	1:1000 (WB)
Mouse IgG anti-OCT3/4	Santa Cruz Biotechnology	Sc-5279	1:60
Rabbit IgG anti-SOX2	Pierce Antibodies	PA1-16968	1:100
Goat IgG anti-NANOG	R&D Systems	AF1997	1:25
Rat IgM anti-SSEA3	Hybridoma Bank	MC-631	1:3
Mouse IgG anti-SSEA4	Hybridoma Bank	MC-813-70	1:3
Mouse IgM anti TRA-1-81	Millipore	MAB4381	1:200
Rabbit IgG anti-alpha-1-fetoprotein	Dako	A0008	1:400
Goat IgG anti-FOXA2	R&D Systems	AF2400	1:50
Rabbit IgG anti-GATA4	Santa Cruz Biotechnology	sc-9053	1:50
Mouse IgG anti SMA	Sigma	A5228	1:400
Mouse IgM anti-ASA	Sigma	A2172	1:400
Mouse IgG anti-TUJ1	Bio Legend	MMS-435P	1:500
Rabbit IgG anti GFAP	Dako	Z0334	1:500
Rabbit IgG anti NF200	Sigma	N4142	1:100
Mouse IgG anti-Nerve growth factor (p75) receptor (ME20.4)	Advanced targeting System	AB-N07	1:100 (IF) 1:1000 (FACS)
Rabbit IgG anti-S100B	Dako	Z0311	1:1000
Mouse IgG anti-AP2	Thermo Scientific	MA1-872	1:50
Rabbit IgG anti-Sox10	Abcam	ac108408	1:50
Mouse IgG anti-MelanA	Ventana	790-2990	1:100
Rabbit IgG anti-MPZ	Abcam	Ab31851	1:500
Rabbit IgG anti-PLP	Abcam	ab28486	1:100
Rabbit IgG anti-GAP43	Novus Biologicals	NB300-143SS	1:500
Mouse IgG anti-Ki67	Santa Cruz Biotechnology	sc-23900	1:50
Mouse IgG anti-HNK1	SIGMA	C6680	1:1000 (FACS)

Extended Methodology

iPSC characterization

Alkaline phosphatase activity was demonstrated using the Alkaline Phosphatase Blue Membrane Substrate Solution (Sigma). Briefly, iPSC were grown on top of mitotically inactivated human foreskin fibroblasts (HFF) during one week. Cells were fixed during 2 min in 3.7% paraformaldehyde and exposed to the substrate solution. After 20 min incubation in the dark, blue staining was evident in iPS colonies. Detection of pluripotency-associated markers (nuclear: OCT4, SOX2 and NANOG; cytoplasmic: SSEA3, SSEA4 and Tra-1-81) was performed on iPSC cultured on HFF for 8 days and fixed with 4% paraformaldehyde (PFA). Then, samples were processed for immunocytochemistry. *In vitro* differentiation ability to the three germ layers was carried out through embryoid body (EB) formation. For endoderm, EBs were plated on 0.1% gelatin (Millipore) coated coverslips and cultured 3 weeks in KODMEM (Gibco) supplemented with 20% fetal bovine serum (Hyclone), 1x penicillin/streptomycin (Gibco), 1x Glutamax (Gibco), 0.05 mM 2-mercaptoethanol (Gibco), non essential aminoacids (Lonza). For mesoderm induction the same medium was used as before mentioned with the addition of 0.5 mM L-ascorbic acid (Sigma). Ectoderm differentiation was done culturing the EBs in suspension in N2B27 medium (Neurobasal:DMEM:F12 50:50 v/v, 1x N2 supplement, 1x B27 supplement, 1x Glutamax) supplemented with b-FGF as described (Sánchez-Danés, 2012). After 10 days in culture, EBs were plated on Matrigel (Corning) coated coverslips and cultured for additional three weeks in N2B27 medium without b-FGF. Differentiated cells were fixed with 4% PFA. Immunocytochemistry was performed by standard methods as previously reported (Martí, 2013). Primary antibodies used are listed in table S5. Secondary antibodies were of the Alexa Fluor series from Jackson Immuno Research and used between 1:250 and 1:500 dilution. Cell nuclei were counterstained with 0.5 µg/ml DAPI (Invitrogen). Images were acquired with an SP5 Leica confocal microscope. For karyotyping, iPSC were cultured on matrigel in the absence of HFF and treated with colcemide (Gibco) at a final concentration of 0.1 µg/mL and processed as described (Campos, 2009).

In the case of retroviral reprogrammed cell lines qPCR was performed to confirm the silencing of the transgenes. Sendai virus reprogrammed iPSC lines were subjected to qualitative PCR to check that they were vector-free at passage 10. The genetic expression of endogenous pluripotency-associated genes (*OCT4*, *NANOG*, *CRIPTO* and *Rex1*) were confirmed by qPCR. Primers employed are listed in Table S4.

For DNA methylation analysis, genomic DNA was extracted from cell pellets using QIAamp DNA Mini Kit (Qiagen 51304). DNA methylation analysis was performed with Methylamp DNA Modification kit (Epigentek P-1001-1) according to manufacturer's specifications. Oct4 and Nanog promoters were amplified by PCR using primers previously described in Freberg et al (2007), amplified in DH5a cells, purified and sequenced. Severe combined immunodeficient (SCID) beige mice (Charles River Laboratories) were used to generate teratomas from two iPSC line, 5PNFiPS(+/-) and 5PNFiPS(-/-). Animal assays were conducted following experimental procedures previously approved by the Institutional Ethics Committee on Experimental Animals, in full compliance with Spanish and European laws and regulations. Teratomas were stained with hematoxylin eosin and also the detection of the three germ layers was done by immunocytochemistry. Antibodies used are included in Table S5.

DNA extraction

Genomic DNA from tumors was extracted using the Gentra Puregene Kit (Qiagen, Chatsworth, CA) following manufacturer's instructions, after tissue homogenization using Tissue Lyser (Qiagen). Genomic DNA from primary cells and iPSCs was extracted using Promega Maxwell 16 system following manufacturer's instructions.

NF1 genetic analysis

NF1 germline and somatic mutations were detected by *NF1* cDNA Sanger sequencing, by gDNA sequencing using the I2HCP NGS custom panel (Castellanos *et al*, 2017) and MLPA from cultured PNF-derived Schwann cells treated with 250 µg/ml puromycin (Sigma) or PNFs DNA following Genetic Diagnostics for Hereditary Cancer Unit protocols. Germline mutations were confirmed by DNA Sanger sequencing from cultured PNF-derived fibroblast cells. Loss of heterozigosity of NF1 locus was detected by Microsatellite multiplex PCR analysis (MMPA) of chromosome 17 (Garcia-Linares *et al*, 2012). Reference sequence used was GeneBank: NG_009018_1, NM_000267_3, NP_000258.1. For intragenic deletions we used GeneBank: NM_001042492.2.

SNP-array analysis

SNP-array analysis was performed on selected samples using Illumina HumanOmniExpress v1 BeadChips (730,525 SNPs). Raw data was processed with Illumina Genome Studio v2011.1 with the Genotyping module v1.9.4 to extract B Allele frequency (BAF) and log R ratio (LRR) and then analyzed with the R package ASCAT (Van Loo *et al*, 2010) to obtain loss of heterozygosity (LOH) and allele specific copy

number (CN) profiles. All samples were analyzed independently and treated as unpaired samples, using the germline genotype prediction functionality from ASCAT.

Exome sequencing

Exome was captured using Agilent SureSelect Human All Exon V5 kit (Agilent, Santa Clara, CA, US) according to the manufacturer's instructions and sequenced in a HiSeq instrument (Illumina) producing 100-base long paired-end reads. Reads were aligned to the hs37d5 reference genome using BWA MEM (Li H 2013) (bwa-0.7.13). After that, duplicates were marked using Picard (v2.0.1) and the Genome Analysis Toolkit (GATK) (McKenna *et al*, 2010) (v.3.4.46) was used for local realignment around indels. GATK's Mutect2 (Cibulskis *et al*, 2013) was used to detect somatic variants specific to primary tumors, SC and iPSC with respect to their associated fibroblasts. Variants were annotated using annovar (Wang *et al*, 2010)(v20160201), filtered using custom R scripts and further validated by manual inspection.

Data visualization

Genomic plots were created with the R/Bioconductor package karyoploteR (Gel & Serra, 2017) and additional custom R scripts. Graphs were created with Graphpad Prism 7.0.

RT-qPCR analysis

Total RNA was extracted from cultured cells using the 16 LEV simplyRNA Purification Kit, from Maxwell technology following manufacturer's instructions. RNA (0,5 µg) was reverse-transcribed using the Superscript III reverse transcriptase enzyme (Life technologies) according to manufacturer's instructions. Quantitative polymerase chain reaction (qPCR) was performed with Roche Universal Probe Library (UPL) technology and analyzed using the Light-Cycler® 480 Real-Time PCR System (Roche Diagnostics). Gene expression was normalized to two selected reference genes (*EP300* and *TBP*) and expressed as Normalized Relative Expression (NRE). Primer sequences used are listed in Table S4. A Microsoft Excel spreadsheet was used to analyze qPCR data for relative expression calculations (Terribas *et al*, 2013).

Western Blotting

Cells were washed with chilled PBS twice and lysed with RIPA buffer (50 mM Tris-HCl (pH 7.4), 150 mM NaCl, 1mM EDTA, 0.5% Igepal CA-630) supplemented with 3mM DTT (Roche), 1mM PMSF (Fluka), 1mM sodium orthovanadate (Sigma), 5mM NaF (Honeywell), 10 ug/ml leupeptin (Sigma), 5ug/ml aprotinin (Sigma) and 1xPhosSTOP (Roche). Lysates were boiled with 1X Laemmli buffer and 90 µg of protein was subjected to SDS-PAGE and transfered onto PVDF membranes (18 hours 90mA at 4ºC). Membranes were blocked with Odyssey Blocking Buffer (PBS)(LI-COR) and incubated with rabbit anti-NF1 Antibody (Bethyl laboratories) at 4ºC overnight; and with mouse anti-αtubulin (Sigma-Aldrich) 1 h at room temperature. Membranes were then incubated with IRDye 680LT and IRDye 800CW secondary antibodies (1:25,000 and 1:15,000, respectively; LI-COR) for 1 h at room temperature and scanned using the Odyssey Infrared Imaging System (LI-COR).

Immunocytochemistry and flow cytometry

For immunofluorescence, cells were fixed in 4% para-formaldehyde in PBS for 15min at RT, permeabilized with 0.1%Triton-X 100 in PBS for 10 min at RT, blocked in 10% FBS in PBS for 15 min at RT and stained with the primary antibodies (Table S4) overnight at 4ºC. Secondary antibodies were Alexa Fluor 488- and Alexa Fluor 568- (Invitrogen). Nuclei were stained with DAPI and images captured using LEICA DMIL6000 and LASAF software. Confocal images from spheres were captured using AxioObserver Z1 Confocal LSM 710, and ZEN Black 2012 software. For flow cytometry assays, cells were dissociated with accutase, resuspended in 0.1% BSA in PBS, incubated for 30 min on ice with unconjugated primary antibody p75 and detected with Alexa Fluor 568-conjugated secondary antibodies, following incubation for 30 min on ice with unconjugated primary antibody Hnk1 and detected with Alexa Fluor 488-conjugated secondary antibodies Cells were analyzed by flow cytometry using BD LSR Fortessa SORP and BD FACSDiva 6.2 software.

Proliferation Assay (Click-iT Edu assay)

Two hundred thousand iPSCs (ES4, FiPS and iPSC) were plated on matrigel-coated 6-well plates, and feeded daily with mTESR medium. After 72h cells were treated with 20 µM EdU for 2 hours, fixed, permeabilized and click labeled with Alexa Fluor 488 azide using Click-iT Plus EdU Flow Cytometry Assay Kits (Thermo Fisher) according to the manufacturer protocol. Cells were also stained with propidium iodide to detect DNA content. Data was collected and analyzed using an BD LSR Fortessa SORP and BD FACSDiva 6.2 software.

Scratch assay

$0.5x10^6$ NC cells were plated onto matrigel–coated 6-well dishes. When cells reached confluence a scratch area was created using a sterile tip. Medium was replaced and migration was measured after 6 and 24 hours. To obtain data in cell migration 9 fields covering the scratch were imaged with a 10x lens at 0, 6 and 24 hours after the scratch. The 9 images were joined using tilescan tool from the LASAF software (Leica).

In vitro Myelination assay

In vitro myelination assay was performed as described in Kim H-S et al (Kim *et al*, 2017) co-culturing Rat Dorsal Root Ganglion (DRG) neurons (Innoprot, Spain) with SCP (7 days differentiation)-FiPS, for 30 days.

Statistical Analyses

Statistical analysis was carried out using GraphPad Prism software v7. For multiple group comparisons, a two-tailed unpaired t test was performed. The number of biological replicates (n) for each experiment and average ± SEM are indicated when applicable, and statistical significance is indicated by *p < 0.05, **p < 0.01, and ***p < 0.001.

References

Campos PB , Sartore RC, Abdalla SN, Rehen SK. Chromosomal spread preparation of human embryonic stem cells for karyotyping E J Vis Exp. 2009 Sep 4;(31)

Castellanos E, Gel B, Rosas I, Tornero E, Santín S, Pluvinet R, Velasco J, Sumoy L, del Valle J, Perucho M, Blanco I, Navarro M, Brunet J, Pineda M, Feliubadaló L, Capellá G, Lázaro C & Serra E (2017) A comprehensive custom panel design for routine hereditary cancer testing: preserving control, improving diagnostics and revealing a complex variation landscape. *Sci. Rep.* **7:** 39348

Cibulskis K, Lawrence MS, Carter SL, Sivachenko A, Jaffe D, Sougnez C, Gabriel S, Meyerson M, Lander ES & Getz G (2013) Sensitive detection of somatic point mutations in impure and heterogeneous cancer samples. *Nat. Biotechnol.* **31:** 213–219

Freberg CT, Dahl JA, Timoskainen S, Collas P. Epigenetic reprogramming of OCT4 and NANOG regulatory regions by embryonal carcinoma cell extract. Mol Biol Cell. 2007 May;18(5):1543-53. Epub 2007 Feb 21.

Garcia-Linares C, Mercadé J, Gel B, Biayna J, Terribas E, Lázaro C & Serra E (2012) Applying microsatellite multiplex PCR analysis (MMPA) for determining allele copy-number status and percentage of normal cells within tumors. *PLoS One* **7:** e42682

Gel B & Serra E (2017) karyoploteR: an R/Bioconductor package to plot customizable genomes displaying arbitrary data. *Bioinformatics***:** 31–33

Kim H-S, Lee J, Lee DY, Kim Y-D, Kim JY, Lim HJ, Lim S & Cho YS (2017) Schwann Cell Precursors from Human Pluripotent Stem Cells as a Potential Therapeutic Target for Myelin Repair. *Stem Cell Reports* **8:** 1714–1726

Martí M, Mulero L, Pardo C, Morera C, Carrió M, Laricchia-Robbio L, Esteban CR, Izpisua Belmonte JC. Characterization of pluripotent stem cells. Nat. Protoc. 2013 Feb;8(2):223-53. doi: 10.1038/nprot.2012.154. Epub 2013 Jan 10.

McKenna A, Hanna M, Banks E, Sivachenko A, Cibulskis K, Kernytsky A, Garimella K, Altshuler D, Gabriel S, Daly M & DePristo MA (2010) The Genome Analysis Toolkit: A MapReduce framework for analyzing next-generation DNA sequencing data. *Genome Res.* **20:** 1297–1303

Sánchez-Danés A, Richaud-Patin Y, Carballo-Carbajal I, Jiménez-Delgado S, Caig C, Mora S, Di Guglielmo C, Ezquerra M, Patel B, Giralt A, Canals JM, Memo M, Alberch J, López-Barneo J, Vila M, Cuervo AM, Tolosa E, Consiglio A, Raya A. Disease-specific phenotypes in dopamine neurons from human iPS-based models of genetic and sporadic Parkinson's disease EMBO Mol Med. 2012 May;4(5):380-95. doi: 10.1002/emmm.201200215. Epub 2012 Mar 8.

Terribas E, Garcia-Linares C, Lázaro C & Serra E (2013) Probe-based quantitative PCR assay for detecting constitutional and somatic deletions in the NF1 gene: application to genetic testing and tumor analysis. *Clin. Chem.* **59:** 928–37

Van Loo P, Nordgard SH, Lingjaerde OC, Russnes HG, Rye IH, Sun W, Weigman VJ, Marynen P, Zetterberg A, Naume B, et al. (2010) Allele-specific copy number analysis of tumors. *Proc. Natl. Acad. Sci.* **107:** 16910–16915

Wang K, Li M & Hakonarson H (2010) ANNOVAR: functional annotation of genetic variants from high-throughput sequencing data. *Nucleic Acids Res.* **38:** e164–e164